An enteric neuron-expressed variant ionotropic receptor detects ingested salts to regulate salt stress resistance

Jihye Yeon[1,3], Laurie Chen[1], Nikhila Krishnan[1,2], Sam Bates[1], Charmi Porwal[1], and Piali Sengupta[1,3]

[1]Department of Biology, Brandeis University, Waltham, MA 02454

[2]Current address: Leica Microsystems Inc., Deerfield, IL 60015

[3]Corresponding authors: P.S.: sengupta@brandeis.edu; J.Y.: jihyeyeon@brandeis.edu

Running title: An enteric neuron-expressed ionotropic receptor regulates salt stress resistance

Keywords: ionotropic receptor; enteric neuron; salt stress; acclimation; *C. elegans*; interoception

ABSTRACT

The detection of internal chemicals by interoceptive chemosensory pathways is critical for regulating metabolism and physiology. The molecular identities of interoceptors, and the functional consequences of chemosensation by specific interoceptive neurons remain to be fully described. The *C. elegans* pharyngeal neuronal network is anatomically and functionally homologous to the mammalian enteric nervous system. Here, we show that the I3 pharyngeal enteric neuron responds to cations via an I3-specific variant ionotropic receptor (IR) to regulate salt stress tolerance. The GLR-9 IR, located at the gut lumen-exposed sensory end of I3, is necessary and sufficient for salt sensation, establishing a chemosensory function for IRs beyond insects. Salt detection by I3 protects specifically against high salt stress, as *glr-9* mutants show reduced tolerance of hypertonic salt but not sugar solutions, with or without prior acclimation. While cholinergic signaling from I3 promotes tolerance to acute high salt stress, peptidergic signaling from I3 during acclimation is essential for resistance to a subsequent high salt challenge. Transcriptomic analyses show that I3 regulates salt tolerance in part via regulating the expression of osmotic stress response genes in distal tissues. Our results describe the mechanisms by which chemosensation mediated by a defined enteric neuron regulates physiological homeostasis in response to a specific abiotic stress.

INTRODUCTION

While foraging for food, animals often encounter toxic substances that adversely affect health and longevity. Consequently, animals have evolved multiple mechanisms to identify and cope with harmful chemicals. A first line of defense involves behavioral avoidance mediated by exteroceptive chemosensory neurons present in olfactory and taste organs (Ferkey et al., 2021; Taruno et al., 2021). If ingested, chemicals in the gastrointestinal tract are detected directly or indirectly by non-neuronal cells, as well as gut-intrinsic enteric neurons and extrinsic sensory afferents, to regulate and maintain metabolic homeostasis (Furness et al., 1999; Miguel-Aliaga et al., 2018; Prescott and Liberles, 2022; Spencer and Hu, 2020). In contrast to the well-described exteroceptive chemotransduction pathways, the molecular mechanisms and functional roles of interoceptive chemosensation remain to be fully described.

Inorganic cations such as Na^+ and Ca^{2+} and related salts are essential for the regulation of a range of physiological processes and are typically attractive at low concentrations (Berridge et al., 2003; Taruno and Gordon, 2023). However, high salt concentrations are harmful (Hunter et al., 2022; Rucker et al., 2018), and are detected by gustatory neurons to drive rejection and avoidance, as well as by interoceptive neurons in multiple organs including the gut and brain to modulate salt and fluid intake (Stocker et al., 2024; Taruno and Gordon, 2023). Although the toxic effects of high salt are generally attributed to osmotic stress, comparisons with cellular responses elicited by equiosmolar sugar solutions suggest that individual hypertonic solutes can be discriminated and their concentrations monitored to regulate different physiological responses (Kinsman et al., 2017; Lamitina et al., 2004; Stocker et al., 2024).

Salt sensation is mediated by a diverse range of molecules across species. These include amiloride-sensitive Na^+ channels in mammals, and an expanded family of variant ionotropic

41 receptors (IRs) in *Drosophila* (Stocker et al., 2024; Taruno and Gordon, 2023). In *Drosophila*,
42 distinct IR protein complexes expressed in different external and internal taste sensilla have been
43 implicated in detecting a range of salt concentrations (Kim et al., 2024; Sang et al., 2024; Taruno
44 and Gordon, 2023). Although IR proteins are encoded by the genomes of all protostomes (Croset
45 et al., 2010), chemosensory roles for these proteins in species beyond insects remain to be
46 definitively established.

47 The nematode *C. elegans* is also attracted to low salt but avoids high salt using a small set
48 of ciliated chemosensory neurons present in sense organs of the head and tail (Ferkey et al.,
49 2021). Exposure to high NaCl rapidly paralyzes and eventually kills worms but prolonged
50 exposure to sub-lethal NaCl concentrations increases tolerance upon subsequent high NaCl
51 exposure (acclimation) (Lamitina et al., 2004). Worms are also paralyzed rapidly in high sucrose
52 concentrations (Lamitina et al., 2004), implying that the effects of high salt are due to hypertonic
53 stress. However, worms survive to different extents on equiosmolar NaCl and sugar suggesting
54 that as in mammals, unidentified salt-specific sensors and pathways may regulate salt stress
55 (Lamitina et al., 2004).

56 Food ingestion in *C. elegans* is primarily driven by the foregut or pharynx (Albertson and
57 Thomson, 1976; Avery and You, 2012). This neuromuscular organ is innervated by a densely
58 interconnected, autonomously functioning network of 20 pharyngeal neurons that exhibit
59 developmental, anatomical, and functional homology to the mammalian enteric nervous system
60 (Albertson and Thomson, 1976; Cook et al., 2020; Vidal et al., 2022). 15/20 of these pharyngeal
61 neurons (henceforth referred to as pharyngeal enteric neurons; PENs) exhibit sensory features,
62 although to date, only two PENs have been shown to respond to bacterial compounds to regulate
63 feeding and foraging (Bhatla and Horvitz, 2015; Rhoades et al., 2019).

64 Here we show that the single I3 PEN in *C. elegans* responds to a range of monovalent
65 and divalent cations and regulates salt stress resistance. Salt detection is mediated by the I3-
66 specific GLR-9 IR-related protein which is both necessary and sufficient for salt responses. Salt
67 sensation by I3 is transmitted via cholinergic and peptidergic signaling to increase tolerance to
68 high salt but not high sugars in unacclimated and acclimated animals, respectively. Salt acts via
69 both GLR-9-dependent and -independent pathways to alter the expression of genes in distal
70 tissues including the epidermis and gut that enable salt stress resistance; misregulation of this
71 gene expression program in *glr-9* mutants likely underlies their salt-sensitivity phenotype.
72 Together, our results identify a chemosensory function of an IR in nematodes, and elucidate how
73 a single enteric neuron detects and relays the presence of ingested cations to counter salt toxicity.
74

75 **RESULTS**

76 **The GLR-9 tuning and GLR-7 co-receptor IRs are co-localized to the gut lumen-exposed**
77 **sensory ending of the I3 pharyngeal enteric neuron**

78 The *C. elegans* genome encodes 15 predicted ionotropic receptors related to glutamate-
79 gated cation channels (Brockie et al., 2001; Hobert, 2013) (Fig. 1a). Of these, seven exhibit
80 features characteristic of variant sensory IRs in insects including amino terminal domains of
81 varying lengths, the lack of canonical glutamate-interacting residues in their ligand binding
82 domains, and loss of highly conserved sequences essential for regulating ion permeability in their
83 pore-forming domains (Benton et al., 2009; Brockie et al., 2001; Croset et al., 2010) (Fig. 1a,
84 Fig. S1a). Examination of the neuronal transcriptome database (Taylor et al., 2021) showed that
85 six of these IR-like genes are exclusively or highly expressed in subsets of PENs (Brockie et al.,
86 2001) (Fig. S1b). In particular, the *W02A2.5* IR gene (henceforth referred to as *glr-9*) is

87 expressed only in the single I3 PEN (Fig. S1b), suggesting that *glr-9* may play a specialized
88 sensory role in this neuron.

89 Consistent with transcriptomics data, an endogenous GFP-tagged GLR-9 fusion protein
90 was expressed only in I3 (Fig. 1b). The GLR-9 fusion protein localized to a structure that is
91 present asymmetrically at the I3 ending and protrudes from the cell surface towards the interior
92 of the animal (Fig. 1b, Movie S1). Reconstruction of the sensory ending of I3 from serial section
93 electron micrographs also showed a structure that is expanded and curved (Fig. 1c, Movie S2)
94 (Albertson and Thomson, 1976; Cook et al., 2020), and that may represent the domain occupied
95 by GLR-9. The internal side of this ending is directly adjacent to and is likely exposed to the
96 pharyngeal lumen (Fig. 1c, Movie S2). However, I3 is not ciliated and does not express ciliary
97 genes (Taylor et al., 2021), leaving open the question of the identity of this structure. We infer
98 that GLR-9 may be positioned in I3 to directly sample ingested molecules present in the
99 pharyngeal lumen.

100 Sensory IRs in insects typically function as heterotetramers comprised of a stimulus-
101 specific tuning receptor and one or more co-receptor(s) that traffic the IR complex to the ciliated
102 endings of sensory neurons (Abuin et al., 2011; Abuin et al., 2019; Ai et al., 2013). Similar to
103 other tuning IRs, GLR-9 does not contain an extended amino-terminal domain (Fig. S1a),
104 suggesting that this IR may also act as a tuning receptor. Among the characterized IR co-
105 receptors, IR25a is deeply conserved in all protostomes and is considered the ancestral
106 chemosensory IR (Croset et al., 2010). The *glr-7* IR25a ortholog in *C. elegans* (Croset et al.,
107 2010) (Fig. 1a) is expressed in a small number of pharyngeal and non-pharyngeal neurons with
108 the highest expression in I3 (Fig. S1b) (Taylor et al., 2021). A GFP-tagged GLR-7 fusion protein
109 expressed in I3 was also localized to the sensory ending of I3 (Fig. 1d). Localization of GLR-9

110 was abolished in *glr-7* mutants and *vice versa* (Fig. 1e). Together, these results suggest that
111 GLR-9 and GLR-7 may comprise a sensory receptor complex in the I3 PEN.
112
113 **GLR-9/GLR-7 are necessary and sufficient to mediate I3 responses to high concentrations**
114 **of monovalent and divalent cations**
115 To determine whether the GLR-9/GLR-7 complex detects chemicals present in the
116 pharyngeal lumen, we surveyed chemosensory stimuli-evoked intracellular calcium dynamics in
117 I3 neurons expressing the GCaMP6s calcium sensor. I3 responded robustly to both bacterial
118 supernatant as well as bacterial growth media (LB: Lysogeny or Luria Broth) alone (Fig. S2a)
119 suggesting that I3 responds to one or more chemical components in LB. Further analyses showed
120 that I3 responded to a range of monovalent and divalent salts including NaCl, NaAc, KPO_4,
121 NH_4Cl, $MgSO_4$, NH_4Ac, KCl, $NaPO_4$, $(NH_4)_2SO_4$, and $CaCl_2$ (Fig. 2a, Fig. S2b). Replacement of
122 Na^+ with N-methyl-D-glucamine (NMDG) in NMDG-Cl^- failed to elicit a response, whereas
123 replacing Cl^- with gluconate in Na^+-gluconate resulted in increased intracellular calcium levels
124 (Fig. 2b, Fig. S2c), suggesting that I3 responds non-selectively to cations. No responses were
125 observed to equiosmolar concentrations of fructose, sorbitol, or glycerol (Fig. 2c, Fig. S2d),
126 indicating that I3 does not respond to high osmolarity.
127 I3 responded largely in a dose-dependent manner to NaCl, NaAc, KPO_4 and NH_4Cl (Fig.
128 2d-g). Responses at higher salt concentrations appeared to be tonic with little to no
129 desensitization, and returned to baseline upon removal of the stimulus (Fig. 2d-h, Fig. S2e). Salt
130 responses were maintained in *unc-13* and *unc-31* mutants which abolish synaptic or
131 neuropeptidergic transmission, respectively (Sieburth et al., 2007; Speese et al., 2007) (Fig. S2f),
132 suggesting that I3 responds to salts cell-autonomously, although we are unable to exclude

133 communication via gap junctions. Salt responses in I3 were also unaltered in animals mutant for
134 the *tax-4* cyclic nucleotide-gated and *osm-9* TRPV channel genes required broadly for
135 chemosensation in the ciliated chemosensory neurons of the head amphid sense organs, as well
136 as in animals mutant for the *che-1* terminal selector transcription factor that specifies the fate of
137 the salt-sensing ASE amphid chemosensory neurons (Fig. S2g) (Etchberger et al., 2007; Ferkey
138 et al., 2021; Uchida et al., 2003). All examined salt responses in I3 were abolished in *glr-9*
139 mutants; responses were restored in *glr-9* mutants upon I3-specific expression of wild-type *glr-9*
140 sequences (Fig. 2h, Fig. S2h). We conclude that GLR-9/GLR-7 mediate I3 responses to a broad
141 range of salts.

142 We next tested whether GLR-9/GLR-7 are also sufficient to confer salt responses onto a
143 non salt-sensing neuron. Misexpression of GFP-tagged GLR-9 with or without GLR-7 in the
144 salt-sensing ASE chemosensory neurons resulted in protein accumulation in the soma and failure
145 to traffic into sensory cilia (Fig. S2i). Reasoning that pathways required for trafficking and
146 localization of sensory IRs may be conserved in PENs, we misexpressed GLR-9 and GLR-7 in
147 the I1 PENs whose distal non-ciliated sensory endings are also apposed to the gut lumen
148 (Albertson and Thomson, 1976; Cook et al., 2020). Co-expression of both proteins but not each
149 protein alone led to localization to the I1 sensory endings similar to the pattern in I3 (Fig. S2j).
150 Although I1 did not respond to NaCl, misexpression of both GLR-9 and GLR-7 in I1 was
151 sufficient to confer responses to NaCl (Fig. 2i). These observations indicate that GLR-9 and
152 GLR-7 are both necessary and sufficient to confer salt responses in PENs.

153

154 **GLR-9-mediated salt sensation promotes salt stress resistance**

155 To examine the functional consequences of I3-mediated salt sensation, we assessed
156 multiple salt-regulated behaviors in *glr-9* mutants. Salt chemotaxis behaviors were examined in
157 microfluidics behavioral arenas which allow analyses of behavioral responses to the same salt
158 concentrations as those used to examine neuronal calcium responses (Albrecht and Bargmann,
159 2011; Khan et al., 2022). Wild-type animals were robustly attracted to a central stripe of 75 mM
160 NaCl but avoided 250 mM NaCl (Fig. S3a). *glr-9* mutants exhibited no defects in either salt
161 attraction or avoidance (Fig. S3a), and also exhibited robust avoidance of high glycerol
162 concentrations (Fig. S3b). *glr-9* mutants also exhibited no defects in pharyngeal pumping
163 frequency in low and high salt concentrations in the presence of bacterial food (Fig. S3c). These
164 observations suggest that salt-sensing by I3 may contribute to organismal responses other than
165 taxis or feeding.
166 *C. elegans* is typically grown on media containing 50 mM NaCl which is considered
167 isotonic. When moved to media containing >500 mM NaCl, animals rapidly lose cell volume,
168 become immotile due to loss of turgor pressure, and eventually die (Choe and Strange, 2007a;
169 Lamitina et al., 2004). Since salt-specific pathways independent of hypertonicity have been
170 proposed to also regulate salt toxicity (Lamitina et al., 2004), we tested the notion that I3-
171 mediated salt sensation regulates high salt tolerance. Wild-type animals became rapidly immotile
172 when transferred from 50 mM NaCl to 500 mM NaCl or high concentrations of other I3-sensed
173 salts including NaAc, NH_4Cl, or KPO_4 (Fig. 3a). *glr-9* mutants were consistently paralyzed more
174 rapidly than wild-type animals when moved from low to high NaCl (Fig. 3b), suggesting
175 decreased salt tolerance. However, *glr-9* mutants did not exhibit enhanced sensitivity to
176 equiosmolar sucrose solutions, (Fig. 3c, Fig. S3d) further highlighting the salt-specificity of I3

177 responses. We conclude that I3 activation specifically by salt is partly protective against acute
178 high salt stress.
179 While animals are highly sensitive to acute salt stress, pre-adaptation to 200–250 mM
180 NaCl for 24 hrs allows *C. elegans* to tolerate subsequent exposure to >500 mM NaCl (Lamitina
181 et al., 2004; Urso et al., 2020). This acclimation is thought to be mediated in part via increased
182 expression of enzymes required for the production of intracellular osmolytes which enable
183 osmotolerance (Choe, 2013; Lamitina et al., 2004; Urso and Lamitina, 2021). We examined
184 whether *glr-9* mutants exhibit reduced salt tolerance even upon acclimation. Wild-type animals
185 pre-exposed to 250 mM NaCl or 250 mM KPO_4 for as little as 3 hrs continued to exhibit normal
186 locomotion and pharyngeal pumping for >30 mins when placed on 500 mM NaCl or 500 mM
187 KPO_4, respectively (Fig. 3d-e). However, a significant fraction of *glr-9* mutants again became
188 immotile within 5-10 mins when placed on high concentrations of either NaCl or KPO_4 (Fig. 3d-
189 e). Acclimation was unaffected in animals mutant for signaling genes required for sensory
190 transduction in ciliated chemosensory neurons (Fig. S3e), indicating that these neurons do not
191 contribute to high salt resistance. Since I3 exhibits responses to multiple salts, we next tested
192 whether acclimation to sub-lethal concentrations of one salt enables tolerance of high
193 concentrations of a different salt. Pre-exposure to 250 mM NaCl was sufficient to partly increase
194 tolerance of wild-type but not *glr-9* mutant animals to 500 mM KPO_4 (Fig. 3f). Taken together,
195 we conclude that GLR-9-dependent salt responses in I3 are necessary for tolerance of high salts
196 in both unacclimated and acclimated conditions.
197
198 **Cholinergic and FLP-6 neuropeptide-mediated signaling from I3 are necessary for high**
199 **salt tolerance under different conditions**

200 Osmoregulatory mechanisms operate in multiple tissues and organs to regulate
201 osmotolerance in *C. elegans* (Choe, 2013; Urso and Lamitina, 2021), suggesting that I3 may
202 signal to one or more of these tissues to regulate salt stress resistance. I3 is a cholinergic neuron
203 and also expresses multiple neuropeptides (Cook et al., 2020; Taylor et al., 2021). Knocking out
204 the *unc-17* vesicular acetylcholine transporter specifically in I3 using Cre-Lox mediated
205 recombination (Huang et al., 2023) resulted in rapid paralysis upon exposure to high salt similar
206 to *glr-9* mutants (Fig. 4a), indicating that cholinergic signaling from I3 is necessary for acute salt
207 tolerance.
208 We next addressed the mechanisms by which GLR-9-mediated signaling contributes to
209 salt acclimation. I3 responses to 500 mM NaCl were similar in animals with or without prior
210 acclimation (Fig. S4a), indicating that acclimation does not alter I3 responses to high salt. Loss
211 of *unc-17* specifically in I3 also did not affect acclimation (Fig. S4b), suggesting that cholinergic
212 signaling from I3 regulates salt tolerance only under unacclimated conditions. Since I3 expresses
213 multiple neuropeptides (Taylor et al., 2021), we next knocked out the *egl-21* carboxypeptidase
214 required for processing of a subset of neuropeptides (Jacob and Kaplan, 2003) specifically in I3
215 using Cre-Lox mediated recombination (Huang et al., 2023) and assessed acclimation. Animals
216 lacking *egl-21* in I3 became immotile more rapidly in high salt similar to *glr-9* mutants following
217 acclimation (Fig. 4b), but responded similarly to wild-type animals upon acute salt challenge
218 (Fig. S4c). We conclude that peptidergic signaling from I3 is required for acclimation and
219 subsequent tolerance of high salt but is not required under conditions of acute salt stress.
220 Neuronal transcriptomics analyses indicate that I3 expresses at least 24 neuropeptide
221 genes at different levels (Taylor et al., 2021). Analyses of salt acclimation phenotypes of a subset
222 of I3-expressed neuropeptides showed that animals mutant for the *flp-6* FMRFamide-like

223 neuropeptide failed to tolerate high salt following acclimation (Fig. S4d-e). The salt tolerance
224 phenotype of *glr-9; flp-6* double mutants was similar to that of each single mutant alone
225 suggesting that these molecules act in a linear pathway to regulate acclimation (Fig. S4e).
226 However, *flp-6* mutants behaved similarly to wild-type animals upon acute high salt exposure
227 (Fig. S4f). Since *flp-6* is expressed in multiple neuron types in addition to I3 (Kim and Li, 2004;
228 Taylor et al., 2021), we confirmed that *flp-6* acts in I3 by knocking out *flp-6* specifically in I3 via
229 Cre-Lox-mediated recombination. Loss of *flp-6* expression specifically in I3 was again sufficient
230 to reduce tolerance of high salt following acclimation similar to the phenotype of *flp-6* global
231 mutants, but did not affect tolerance in an acute high salt challenge (Fig. 4c, Fig. S4f). FLP-6 has
232 been shown to interact with multiple candidate neuropeptide receptors that are expressed broadly
233 in neuronal and non-neuronal cells (Beets et al., 2023). However, mutations in single candidate
234 receptor genes had minor or no effects on salt acclimation (Fig. S4g) suggesting that FLP-6
235 receptors may act redundantly within a single cell or across multiple cell/tissue types to regulate
236 salt tolerance. Together, these results indicate that FLP-6-mediated signaling from I3 is
237 necessary to promote tolerance of high salt following acclimation.
238 We next examined the temporal requirement for neuropeptide signaling from I3 to
239 regulate salt tolerance following acclimation. To temporally modulate neuropeptide release from
240 I3, we expressed the auxin receptor TIR1 specifically in I3 in a strain in which the *unc-31* CAPS-
241 related protein required for dense core vesicle fusion (Speese et al., 2007) is endogenously
242 tagged with degron sequences (Cornell et al., 2022; Nishimura et al., 2009; Zhang et al., 2015).
243 Addition of exogenous auxin to the growth plates during acclimation and exposure to high salt
244 resulted in rapid paralysis further supporting the necessity of peptidergic signaling from I3 for
245 tolerance of high salt (Fig. 4d). Addition of auxin only during the 3 hr acclimation period but not

246 during high salt exposure was sufficient to induce rapid paralysis (Fig. 4d), indicating that
247 peptidergic signaling from I3 is necessary only during the acclimation period to promote high
248 salt tolerance. Taken together, our results indicate that cholinergic signaling from I3 increases
249 tolerance of acute salt stress (Fig. 4e). In contrast, FLP-6 neuropeptide signaling from I3 during
250 acclimation is protective in response to subsequent high salt exposure (Fig. 4e).
251
252 **Salt acclimation alters gene expression via both GLR-9-dependent and -independent**
253 **pathways**
254 The rapidity with which *C. elegans* loses fluid and paralyzes in hypertonic solutions is in
255 part determined by the permeability of the animal's cuticle as well as the concentration of
256 internal osmolytes. Consistently, increased salt resistance following acclimation occurs as a
257 consequence of altered expression of molecules such as cuticular collagens and osmolyte
258 biosynthetic enzymes predicted to be protective against hypertonicity (Burkewitz et al., 2012;
259 Dodd et al., 2018; Lamitina et al., 2004; Lamitina et al., 2006; Rohlfing et al., 2010). We
260 hypothesized that I3 signaling regulates the expression of a subset of genes in distal tissues such
261 as the cuticle, epidermis and gut that contribute specifically to salt tolerance, and that failure to
262 correctly regulate these genes in *glr-9* mutants contributes to their decreased salt resistance. To
263 test this notion, we compared the transcriptional profiles of wild-type and *glr-9* mutants prior to
264 and following 3 hrs of salt acclimation (Fig. 5a-b).
265 Principal component analyses indicated that transcriptional profiles clustered based on
266 both genotype and condition (Fig. S5a). Comparison of the transcriptional profiles of wild-type
267 animals prior to and following acclimation identified 92 and 33 significantly up- and down-
268 regulated genes, respectively (Fig. 5a, Data Table 1). A small subset of these differentially

269 expressed genes overlapped with those identified previously using partly distinct experimental
270 conditions (Dodd et al., 2018; Rohlfing et al., 2011) (Fig. S5b). Consistent with previous
271 observations, the *gpdh-1* and *gpdh-2* glycerol-3-phosphate dehydrogenase, *pgph-2*
272 phosphoglycolate phosphatase, and *tre-5* trehalase encoding genes were upregulated following
273 acclimation (Fig. 5a,c, Data Table 1). Transcriptional upregulation of these enzymes upon
274 hypertonic stress contributes to the production of the osmolyte glycerol which is protective for
275 hypertonic stress (Dodd et al., 2018; Lamitina et al., 2004; Lamitina and Strange, 2005; Possik et
276 al., 2022; Rohlfing et al., 2011). The expression of a subset of genes encoding collagen was also
277 altered consistent with a role for cuticular components in regulating hypertonic stress responses
278 (Fig. 5a,d, Data Table 1) (Choe, 2013; Dodd et al., 2018; Lamitina et al., 2006; Rohlfing et al.,
279 2011; Solomon et al., 2004; Urso and Lamitina, 2021; Wheeler and Thomas, 2006; Wimberly
280 and Choe, 2022).

281 Acclimation resulted in altered expression of a larger set of genes in *glr-9* mutants (Fig.
282 5b, Data Table 1). However, the expression of *gpdh-1*, *pgph-2* and *tre-5* was no longer
283 significantly altered in *glr-9* mutants (Fig. 5b-c, Data Table 1), indicating that I3-mediated
284 signaling in response to salt is necessary for the upregulation of these enzymes. Although a
285 subset of genes including genes encoding cuticular collagens was regulated similarly in both
286 wild-type and *glr-9* mutants following acclimation (Fig. 5e, Data Table 1), the expression of
287 distinct sets of genes implicated in stress responses and in the regulation of metabolism, as well
288 as genes are predicted to encode components of the cuticle or hypodermis, was altered in
289 acclimated *glr-9* mutants (Fig. 5b,d, Fig. S5c, Data Table 1). We conclude that altered gene
290 expression upon salt acclimation is mediated via both I3-dependent pathways that may be salt-
291 specific, and I3-independent pathways that may respond to general hypertonic stress.

292 We noted that the transcriptional profile of *glr-9* mutants was distinct from those of wild-
293 type animals even at 50 mM NaCl (Fig. 5c-d, Fig. S5a,d, Data Table1) suggesting that chronic
294 I3-mediated signaling may be necessary for regulating physiology even at isotonic salt
295 concentrations. Significantly upregulated genes in *glr-9* mutants included genes implicated in the
296 regulation of metabolism and stress, multiple components of the cuticle and hypodermis
297 including collagen and chitinase-like genes, as well as nematode-specific groundhog-like (GRL)
298 and ground-domain (GRD) secreted proteins that are apical extracellular matrix components of
299 the cuticle and precuticle (Hao et al., 2006; Serra et al., 2024) (Fig. 5b,d, Fig. S5d, Data Table 1).
300 These observations suggest that chronic *glr-9* signaling under standard growth conditions may
301 signal the presence of salt, and that the cuticular barrier may be structurally remodeled in the
302 absence of this signaling, potentially contributing to the decreased resistance of these animals to
303 acute salt stress (see Discussion).
304 To assess the functional significance of these expression changes, we tested two
305 predictions arising from the transcriptional profiling data. Animals moved from 50 mM NaCl to
306 either 400 mM or 500 mM NaCl exhibit similar initial responses including rapid shrinkage and
307 paralysis (Choe, 2013; Choe and Strange, 2007a). However, while prolonged exposure to 500
308 mM NaCl leads to death (Lamitina et al., 2004; Solomon et al., 2004), animals regain body
309 volume and motility after 2-4 hrs on 400 mM NaCl via modulation of ion transport and
310 upregulation of osmotolerance genes (Choe and Strange, 2007a, b). The failure of *glr-9* mutants
311 to upregulate osmotolerance genes and their extensively remodeled cuticle even under isotonic
312 conditions predicts that these animals will be unable to recover, or will recover more slowly, on
313 400 mM NaCl. Consistent with this prediction, we found that *glr-9* mutants regained motility
314 significantly more slowly than wild-type animals under these conditions (Fig. S6a). These results

315 further support the notion that I3 signaling-regulated gene expression changes play a critical role
316 in regulating salt tolerance.

317 The finding that salt acclimation results in gene expression changes that are partly I3-
318 dependent and are thus salt-specific, also predicts that different hypertonic solutions may alter
319 the expression of different gene subsets, with only a shared subset being regulated by general
320 osmotic stress. This hypothesis predicts that acclimation to high salt would not be protective in
321 response to high sugar challenge and *vice versa*. We found that acclimation to 250 mM NaCl did
322 not increase tolerance of either wild-type or *glr-9* mutants to 500 mM sucrose, and conversely,
323 acclimation to 250 mM sucrose had no effect on resistance to 500 mM NaCl under our
324 experimental conditions (Fig. S6b). We infer that partly distinct pathways contribute to the
325 detection of individual hypertonic solutes to regulate specific organismal stress responses.
326

327 **DISCUSSION**

328 Here we show that salt-sensing by the single I3 enteric neuron specifically promotes salt
329 stress resistance in *C. elegans.* I3 salt responses are dependent on the GLR-9/GLR-7 IR proteins
330 which are both necessary and sufficient for salt detection. I3 signals via cholinergic and
331 peptidergic signaling to increase salt stress resistance in unacclimated and salt-acclimated
332 animals, respectively. We find that signaling from I3 modulates the expression of genes that
333 regulate cuticle composition and internal osmolyte concentration, resulting in tolerance of high
334 salts but not high sugars (summarized in Fig. 5f). Our observations describe the molecular and
335 neuronal mechanisms by which chemosensation by an enteric neuron regulates physiological
336 homeostasis in response to a specific abiotic stress.

337 Chemoreceptors are among the fastest evolving gene families in multicellular animals,
338 with some gene families being entirely lost or gained within specific lineages (Policarpo et al.,
339 2024; Sanchez-Gracia et al., 2009; Valencia-Montoya et al., 2024). For example, while variant
340 IR sensory proteins are found in all protostomes, they are absent from deuterostomes (Croset et
341 al., 2010; Valencia-Montoya et al., 2024). However, to date, chemosensory roles for these IR
342 proteins have been described and/or suggested primarily in arthropods (Benton et al., 2009; Eyun
343 et al., 2017; Graeve et al., 2022; Groh-Lunow et al., 2014; Ni, 2020). Our identification of a
344 chemosensory function of an IR in *C. elegans* implies that IRs may have retained chemosensory
345 functions in the protostome lineage through evolution. It remains to be determined whether the
346 remaining PEN-expressed IRs in *C. elegans* also function as chemosensors, or whether similar to
347 some *Drosophila* and mosquito IRs (Ni, 2020; van Giesen and Garrity, 2017), subsets of these
348 proteins also detect other sensory cues.
349 GLR-9-mediated salt sensation is transmitted via distinct signaling pathways from I3 to
350 modulate gene expression in tissues and organs such as the gut and cuticle to enhance salt
351 tolerance. We find that even under isotonic conditions, *glr-9* mutants exhibit broad changes in
352 the expression of genes that may impact hypertonic salt resistance. Since I3 responds tonically to
353 a range of salt concentrations, we propose that chronic activation of GLR-9 and cholinergic
354 signaling from I3 upon growth on low salt enhances resistance to acute high salt. Remodeling of
355 the cuticle in the absence of I3 signaling may thus sensitize animals to high salt stress, resulting
356 in more rapid paralysis upon an acute high salt challenge (Fig. 5f). During acclimation, FLP-6-
357 mediated signaling from I3, as well as from other neuronal and non-neuronal osmosensory
358 pathways, drive broad gene expression changes that promote salt tolerance. The failure to alter
359 the expression of a subset of these genes, including osmolyte biosynthesis genes, in acclimated

360 *glr-9* mutants, along with their dysregulated gene expression under isotonic conditions, may
361 underlie their decreased salt tolerance phenotype (Fig. 5f). Additional pathways likely also
362 contribute to osmotolerance under different conditions and timepoints following stress exposure
363 (Huang et al., 2007; Igual Gil et al., 2017; Lee et al., 2016).

364 While exposure to hypertonic solutions can cause general effects such as altered protein
365 quality control and tissue deformation (Burkewitz et al., 2011; Choe and Strange, 2008; Lamitina
366 et al., 2006; Urso and Lamitina, 2021), several lines of evidence including our findings suggest
367 that *C. elegans* and other animals can discriminate among different hypertonic solutes. First,
368 equiosmolar concentrations of salt and sucrose result in distinct survival rates in *C. elegans*
369 (Chandler-Brown et al., 2015; Choe and Strange, 2007a; Lamitina et al., 2004), implying that
370 individual osmotic stressors can elicit partly different organismal responses. Second, *glr-9*
371 mutants exhibit decreased tolerance of high salts but not equiosmolar sugar, highlighting the salt-
372 specificity of the I3 pathway. Third, acclimation to NaCl does not confer resistance to sucrose
373 and *vice versa* under our experimental conditions (see (Chandler-Brown et al., 2015)), indicating
374 that the adaptive response to one osmotic stressor is not fully sufficient to protect against others.
375 Fourth, hypertonic salt regulates the expression of a subset of osmotolerance genes in a GLR-9-
376 dependent manner, further suggesting the presence of solute-specific pathways. Similarly, in
377 rodents, while a number of physiological responses are independent of hyperosmotic solute
378 identity, arterial blood pressure regulation and sympathetic nerve activity are more sensitive to
379 central NaCl infusion than to equiosmolar sugars (Kinsman et al., 2017). Moreover, subsets of
380 OVLT neurons in the circumventricular organs of the brain preferentially respond to hypertonic
381 NaCl over equiosmolar sugars (Kinsman et al., 2017; Stocker et al., 2024), indicating the
382 existence of NaCl-specific, non-osmosensory pathways. Given the critical role of salts in

383 regulating physiological processes, we suggest that dedicated neuronal pathways for high salt
384 detection provides additional flexibility in coordinating responses based on internal state.
385 Enteric sensory neurons in *C. elegans* appear to utilize partly distinct sensory
386 mechanisms from those of somatic exteroceptive sensory neurons. For instance, the GUR-3
387 gustatory receptor-like protein required for hydrogen peroxide detection by the I2 PEN in *C.*
388 *elegans*, and the DEL-3 and DEL-7 ASIC channels that detect ingested bacteria in the NSM PEN
389 are expressed exclusively or primarily in PENs (Bhatla and Horvitz, 2015; Rhoades et al., 2019;
390 Taylor et al., 2021). Similarly, 6 of the 7 IRs including GLR-7 and GLR-9 are expressed
391 primarily or highly in PENs. Moreover, PENs are non-ciliated unlike exteroceptive sensory
392 neurons, suggesting novel mechanisms for receptor trafficking and localization at their sensory
393 endings. The intrinsic enteric neuronal network has ancient evolutionary origins and is thought to
394 have arisen prior to and independently of the central nervous system (Furness and Stebbing,
395 2018; Watanabe et al., 2009). Investigating the mechanisms underlying enteric neuron
396 development and function in diverse organisms may provide insights into ancestral neuronal
397 strategies, and expand our understanding of interoceptive sensory functions across species.
398

399 **METHODS**

400 **Growth of *C. elegans* strains**

401 *C. elegans* strains were grown on NGM plates seeded with *E. coli* OP50 at 20˚C. *unc-*
402 *122*p*::dsRed* or *gfp* were used as co-injection markers (at 40 ng/µl) to generate transgenic strains.
403 Strains were generated using standard genetic crosses. The genotypes of all strains were verified
404 by sequencing or phenotypic examination. All experiments were performed using young adult

405 hermaphrodites grown under well-fed conditions for at least three generations. A list of all
406 strains used in this work is provided in Table S1.
407
408 **Molecular biology**
409 1.1 kb of sequences upstream of and including the *glr-9* START codon were amplified
410 from wild-type animal lysate and used to drive expression specifically in I3. Expression in I1
411 was driven using 1.1 kb of sequences upstream of the *lgc-8* START codon. GLR-9 cDNA was
412 amplified from wild-type animal lysate and tagged with *gfp* for localization and for functional
413 rescue experiments. Since *glr-7* has *a* and *b* isoforms, the genomic region of *glr-7* from the
414 START codon of the *b* isoform (X: 2,419,477) to the STOP codon of both *a* and *b* isoforms
415 (X:2,414,064) was amplified from wild-type animal lysate. These sequences were tagged with
416 *TagRFP* to examine localization of *glr-7*. All plasmids were generated using standard cloning
417 methods and verified by Sanger sequencing. A list of plasmids used in this work is provided in
418 Table S2.
419
420 **CRISPR/Cas9-mediated genome editing**
421 Deletion alleles of *glr-9* and *osm-9* were generated using an injection mix containing 0.5
422 µl of Cas9 (IDT), 1.5 µl of 100 µM tracrRNA, 1 µl of 50 µM 5'-crRNA, 1 µl of 50 µM 3'-
423 crRNA, 1 µl of 17 µM *dpy-10* crRNA as a co-CRISPR injection marker, and nuclease-free water,
424 for a total volume of 10 µl. No DNA donor was used. Worms were maintained at 25°C after
425 injection. Three days following injection, dumpy or roller F1 progeny were segregated onto
426 individual plates. After the singled F1 animals laid eggs, parents were lysed and genotyped using
427 PCR.

428 To generate the *flp-6::loxP* insertion strain (PY12288, Table S1), the injection mix
429 included 0.5 µl of Cas9 (IDT), 2.8 µl of 34 µM crRNA, 0.2 µl of 100 µM tracrRNA, 2 µl of 26
430 µM donor DNA, 50 ng/µl of column-purified *unc-122*p*::gfp*, and nuclease-free water for a total
431 volume of 20 µl. Following injection, worms were kept at 25°C. F1 progeny carrying the *unc-*
432 *122*p*::gfp* co-injection marker were singled onto individual plates and genotyped. The C-
433 terminal *loxP* site was inserted first, followed by insertion of the N-terminal *loxP* site. All
434 tracrRNA, crRNAs, and donor DNAs were obtained from IDT. The sequences of the crRNAs
435 and donor DNA are listed below.

glr-9 *(oy180)*	crRNA #1	5'- atatgcacttttcattcaat -3'
	crRNA #2	5'-ccacattgtgaaatctttac-3'
osm-9 *(oy202)*	crRNA #1	5'- ttttttcagaaaccaaacat-3'
	crRNA #2	5'–acactttgtgtaccatactt-3'
flp-6::loxP *(oy203)*	crRNA #1 (N-terminal *loxP*)	5'-cttattgaacaccatggcaa-3'
	crRNA #2 (C-terminal *loxP*)	5'-cttcgtttccttcgattgat-3'
	Donor #1 (N-terminal *loxP*)	5' - ccgtaatttttgtaagtaaaaagagacattcgtttttcaataacttcgtatagcatacattata cgaagttatcttattgaacaccatggcaatgagatactagtttccgctgatttgtgatattttc cctttgattgaaaac - 3'

	Donor #2 (C-terminal *loxP*)	5' - gtaaacctacacttttaatccctactttttacaattctactagtcccatataacttcgtatagc atacattatacgaagttatactcttcgtttccttcgattgataaagttttgcaccgtgtttttca cacagaatcacctcttttatc -3'

436

437 **Phylogenetic analysis**

438 iGluR sequences from *Mus musculus* and *Drosophila melanogaster* were obtained from
439 Croset et al (Croset et al., 2010). iGluR and IR sequences from *C. elegans* were obtained from
440 Wormbase (www.wormbase.org). Sequences were aligned using MUSCLE (Edgar, 2004), and a
441 phylogenetic tree was constructed using the Maximum Likelihood method with adaptive
442 bootstrapping (116 replicates) in MEGA 12.0.9. The resulting tree was visualized and modified
443 using FigTree v1.4.4.

444

445 **Fluorescent reporter imaging**

446 1 day-old adult animals were anesthetized with 10 mM (-)- tetramisole hydrochloride
447 (Sigma-Aldrich L9756) and mounted on 10% agarose pads on microscope slides. Images in
448 Figure 1b,d, Fig. S2i were acquired at 0.2 µm *z*-intervals using a 100× oil immersion objective
449 on an inverted two- camera spinning disk confocal microscope (Leica DMI6000B with a CSU-
450 W1 spinning disk head and two Andor Neo sCMOS cameras) and Andor IQ3.5 Software. Images
451 in Figure 1e and Fig. S2j were acquired using a 64× oil immersion objective on an inverted
452 spinning disk confocal microscope (Zeiss AxioObserver with Yokogawa CSU-X1 confocal head
453 system and QuantEM SC512 camera) and SlideBook™ software. All images were processed
454 using FIJI/Image J.

455

456 **3D reconstruction of I3 sensory ending**

457 Serial section electron microscope (EM) images of I3 were obtained from Wormimage
458 (www.wormimage.org). I3 was identified as "blue 14" on the EM images (with the assistance of
459 David Hall), specifically from the sections N2T_114522 to N2T_114583. The TrakEM2 plugin
460 in Fiji was used for manually aligning I3 images. Following the alignment, manual segmentation
461 was performed using 3dmod v4.11 from the IMOD suite (https://bio3d.colorado.edu/imod/) to
462 generate the 3D reconstruction of the I3 sensory ending.

463

464 **Acute salt stress assay**

465 Acute responses to high salt were examined using a protocol adapted from (Rohlfing et
466 al., 2010). 6 cm unseeded NGM plates supplemented with the indicated salt concentrations were
467 divided into two sections to assess the behaviors of wild-type and *glr-9* mutant in parallel.
468 Growth-synchronized 1-day old adult hermaphrodites were transferred from NGM plates
469 containing 50 mM NaCl to high salt-containing plates to initiate the assay. Each assay included
470 10 animals of each genotype, and the time at which all 10 animals were unresponsive to touch
471 with a platinum wire was recorded. Unresponsive was defined as failure to move upon prodding
472 with a platinum wire at the nose and tail, and cessation of pharyngeal pumping. At least three
473 independent assays were conducted over multiple days for each data point.

474

475 **Salt acclimation assay**

476 Acclimation experiments were performed using an adaptation of a previously published
477 protocol (Rohlfing et al., 2010). 35 growth-synchronized 1-day adult hermaphrodites were

478 transferred from NGM growth plates (50 mM NaCl) to NGM plates containing 250 mM NaCl,
479 250 mM KPO_4, or 250 mM sucrose and seeded with 200 µl *E. coli* OP50. Animals were
480 maintained at 20˚C for 3 hrs. Following 3 hrs of acclimation, animals were transferred to
481 unseeded plates containing 500 mM NaCl, 500 mM KPO_4, or 500 mM or 1 M sucrose, and
482 tested for responses upon prodding with a platinum wire after 5, 10, 15 and 30 mins.
483 Unresponsive was defined as failure to move upon prodding with a platinum wire at the nose and
484 tail, and cessation of pharyngeal pumping. At least three independent assays were conducted
485 over multiple days for each data point.
486
487 **Salt recovery assay**
488 Recovery from paralysis on 400 mM NaCl was examined using an adaptation of
489 previously published protocols (Choe and Strange, 2007a; Lamitina et al., 2004). Bacteria-
490 seeded growth plates were supplemented with 400 mM NaCl and divided into two sections to
491 assess wild-type and *glr-9* animals in parallel. Growth-synchronized 1-day old adult
492 hermaphrodites were transferred from growth plates containing 50 mM NaCl to the assay plates
493 and were examined every 15 mins up to 4 hrs. Each assay included 10 animals of each genotype.
494 Unresponsive was defined as failure to move upon prodding with a platinum wire at the nose and
495 tail, and cessation of pharyngeal pumping. At least three independent assays were conducted
496 over multiple days for each data point.
497
498 **Glycerol avoidance assay**
499 The avoidance assay was performed as previously described (Culotti and Russell, 1978).
500 Briefly, a ring of 8M glycerol with xylene cyanol (Sigma-Aldrich X4126) was pipetted onto an

501 unseeded NGM plate dried overnight. For each assay, 10 one-day-old adult hermaphrodites were
502 transferred to the center of the glycerol ring. After 10 mins, the number of animals inside and
503 outside the ring was counted. Wild-type and *glr-9*(*oy180)* mutants were examined in parallel.
504

505 **Auxin-induced degradation**

506 400 mM Auxin [1-naphthaleneacetic acid (NAA), Sigma 317918)] was dissolved in
507 EtOH and added to NGM containing the indicated salt concentrations to make 4 mM auxin-
508 containing plates. Control plates contained equal concentrations of EtOH alone. Plates were
509 seeded with 100 µl *E. coli* OP50, dried overnight, and stored at 4˚C wrapped in aluminum foil to
510 prevent light exposure.

511 At least 70 young adult hermaphrodites were transferred from NGM growth plates to
512 plates containing 250 mM NaCl supplemented with either auxin or ethanol. After 3 hrs
513 acclimation, animals were tested for movement on plates containing 500 mM NaCl
514 supplemented with either auxin or ethanol. Animals were examined at 5, 10, 15, and 30 mins for
515 responses to touch with a platinum wire. Each assay included 30 animals per condition and per
516 genotype and was conducted over multiple days. At least 2 sets of experiments were performed
517 for each genotype on the same day. Experimental and control strains were examined together in
518 the same assays in each experiment.
519

520 **Quantification of pumping frequency**

521 Pumping frequency was measured manually using 1-day old adult animals on OP50-
522 seeded NGM plates containing 50 mM or 250 mM NaCl. For each data point, the pumping
523 frequency of individual animals was measured three times for 20 sec each to obtain the average

524 pumping frequency. Wild-type and *glr-9* mutants were examined together in the same assays for
525 each experiment. At least three independent assays were conducted over multiple days for each
526 data point.
527
528 **Microfluidics behavioral assay**
529 Behavioral assays using microfluidics devices were performed essentially as previously
530 described (Khan et al., 2022). After degassing the assembled microfluidic devices, the outlet port
531 was loaded with 5% v/v poloxamer surfactant (Sigma P5556) containing 2 mg/ml xylene cyanol
532 to eliminate bubbles. 20 to 30 1-day old adult hermaphrodites were transferred to unseeded
533 NGM plates, washed with water, and loaded into two separate arenas within a single device. *glr-*
534 *9* mutants were assessed in the same device, with wild-type controls placed in the adjacent arena.
535 After allowing the worms to disperse (<5 min), the stimulus flow containing either 75 mM NaCl
536 or 250 mM NaCl and 2 mg/ml xylene cyanol for visualization was initiated. 20 min videos were
537 recorded at 2 Hz using a PixelLink camera. Microfluidic devices were cleaned after each
538 experiment by washing with water and 100% ethanol before reuse. Custom MATLAB software
539 was used to process and analyze all recordings, and data were visualized using custom R scripts
540 (https://doi.org/10.5281/zenodo.13748735). Mean residency histograms and chemotaxis indices
541 were analyzed as previously described (Khan et al., 2022). Three independent assays were
542 performed over multiple days.
543
544 **Calcium imaging**
545 Custom microfluidic devices for calcium imaging were fabricated as described previously
546 (Khan et al., 2022). Images were acquired using an Olympus BX52WI microscope with a 40× oil

547 objective and a Hamamatsu Orca CCD camera at 4 Hz with 4 × 4 binning. All stimuli were
548 diluted in filtered Milli-Q water, and animals were paralyzed with 10 mM (-)-tetramisole
549 hydrochloride (Sigma L9756) dissolved in water prior to loading on the unseeded NGM. Stimuli
550 dilutions were prepared fresh in water on the day of each imaging session. Responses to 30 sec
551 of water, 30 sec of stimuli, and 30 sec of water were recorded in I3. Data were collected from
552 biologically independent experiments conducted over at least two days. For GCaMP
553 fluorescence analysis, recorded videos were processed using Fiji as previously described (Khan
554 et al., 2022). Briefly, images were aligned using the Template Matching plugin, and cell body
555 and background fluorescence were calculated using manually drawn ROIs. Background-
556 subtracted fluorescence intensity values were used for analysis in R Studio. The baseline
557 fluorescence intensity (F_0) was calculated as the average $\Delta F/F_0$ value over 5 sec prior to stimulus
558 onset. R Studio was used to compute the response mean and SEM
559 (https://doi.org/10.5281/zenodo.13748735). Peak $\Delta F/F_0$ values were calculated as the maximum
560 change in fluorescence relative to F_0 within 10 sec following stimulus addition.
561

562 **RNA-Seq**

563 Animals were synchronized by bleaching adults, collecting eggs, and then arresting
564 hatched L1s in the absence of food for ~16 hours. ~1,000 animals were cultured on *E. coli* OP50
565 seeded at 1 ml per 10 cm plate at 20˚C until the 1 day-old adult stage. Animals from a total of
566 four 10 cm plates were used per sample. Animals were washed with M9 containing 0.01% Triton
567 (Sigma T8787) and placed onto either 10 cm OP50 seeded NGM plates or NGM plates
568 supplemented with 250 mM NaCl for 3 hrs at 20˚C. Animals were then washed off the plates
569 with M9 containing 0.01% Triton. Total RNA extraction was performed using TRIzol

570 (Invitrogen 15596026) and chloroform (Sigma 288306), followed by RNA Clean &
571 Concentrator™-5 (Zymo Research R1014) to extract total RNA. The quality and concentration
572 of total RNA was assessed using Agilent High Sensitive RNA ScreenTape analysis (Agilent
573 5067-5579).

574 100 ng/µl of total RNA per sample was used as input to generate a sequencing library
575 using the xGen™ Broad Range RNA library preparation Kit (IDT 10009865) with AMPure XP
576 Beads (Beckman Coulter A63880). Agilent DNA ScreenTape (D1000 5067-5582) assays were
577 used to assess the quality of the library prior to sequencing. Libraries were paired-end sequenced
578 at 75x75 bases on a NextSeq 1000 system (Illumina). Sequencing reads were adapter trimmed
579 using Trim Galore (https://doi.org/10.5281/zenodo.7598955), mapped to the WBcel235 *C.*
580 *elegans* genome, and counted using STAR (Dobin et al., 2013) with alignMatesGapMax 2500.
581 Differential expression analysis was performed in R studio with DESEQ2 (Love et al., 2014)
582 (BioProject accession number PRJNA1227491). The PCA, heatmaps, and volcano plots were
583 generated using the ggplot package in R. Venn diagrams were created using VennDiagram in R.
584 GO terms, Wormbase, WomCat, Uniprot, and PANTHER were used to categorize individual
585 genes listed in Data Table 1.
586

587 **Statistical analyses**

588 Statistical analyses were performed using Prism v10.4.1. Comparisons to wild-type were
589 performed with t-test or one-way ANOVA across the genotype and condition unless indicated
590 otherwise. Corrections for multiple comparisons were performed using Dunnett's tests. Scatter
591 plots and bar graphs were generated and analyzed using Prism 10. The statistical tests used,

592 significance values, and the number of animals and assays are indicated in the legend to each
593 Figure.
594
595 **Data availability**
596 Underlying data for all behavioral and calcium imaging experiments have been deposited
597 to Figshare. All other data necessary for confirming the conclusions of this article are
598 represented fully within the article and its tables and figures.
599
600 **Acknowledgements**
601 We are grateful to David Hall for assistance with identification of I3 in electron
602 microscopy serial sections, Kirsten Judge for assistance with imaging, and Evelyn Keefer,
603 Gillian Berglund, and Katherine Abruzzi for help with RNA-Seq experiments. We thank Todd
604 Lamitina, Steven Flavell, Ugur Dag, and Yung-Chi Huang for discussion and advice, and Paul
605 Garrity, Steven Flavell, Nathan Harris, Todd Lamitina, Stephen Nurrish, and Alison Philbrook
606 for critical comments on the manuscript. A subset of strains was obtained from the
607 *Caenorhabditis* Genetics Center and the National BioResource Project (Japan). This work was
608 funded in part by the NIH (R35 GM122463 – P.S., T32 MH 19929 – L.C., T32 GM139798 and
609 F31 NS134251 – S.B.) and the NSF (IOS 2042100 – P.S.).
610

611 **REFERENCES**
612

613 Abuin, L., Bargeton, B., Ulbrich, M.H., Isacoff, E.Y., Kellenberger, S., and Benton, R. (2011).
614 Functional architecture of olfactory ionotropic glutamate receptors. Neuron *69*, 44-60.
615 Abuin, L., Prieto-Godino, L.L., Pan, H., Gutierrez, C., Huang, L., Jin, R., and Benton, R. (2019).
616 In vivo assembly and trafficking of olfactory Ionotropic Receptors. BMC Biol *17*, 34.
617 Ai, M., Blais, S., Park, J.Y., Min, S., Neubert, T.A., and Suh, G.S. (2013). Ionotropic glutamate
618 receptors IR64a and IR8a form a functional odorant receptor complex in vivo in
619 *Drosophila*. J Neurosci *33*, 10741-10749.
620 Albertson, D.G., and Thomson, J.N. (1976). The pharynx of *Caenorhabditis elegans*. Phil.
621 Transact. R. Soc. Lond. B *275*, 299-325.
622 Albrecht, D.R., and Bargmann, C.I. (2011). High-content behavioral analysis of *Caenorhabditis*
623 *elegans* in precise spatiotemporal chemical environments. Nat Methods *8*, 599-605.
624 Avery, L., and You, Y.J. (2012). *C. elegans* feeding. WormBook, 1-23.
625 Beets, I., Zels, S., Vandewyer, E., Demeulemeester, J., Caers, J., Baytemur, E., Courtney, A.,
626 Golinelli, L., Hasakiogullari, I., Schafer, W.R.*, et al.* (2023). System-wide mapping of
627 peptide-GPCR interactions in *C. elegans*. Cell Rep *42*, 113058.
628 Benton, R., Vannice, K.S., Gomez-Diaz, C., and Vosshall, L.B. (2009). Variant ionotropic
629 glutamate receptors as chemosensory receptors in *Drosophila*. Cell *136*, 149-162.
630 Berridge, M.J., Bootman, M.D., and Roderick, H.L. (2003). Calcium signalling: dynamics,
631 homeostasis and remodelling. Nat Rev Mol Cell Biol *4*, 517-529.
632 Bhatla, N., and Horvitz, H.R. (2015). Light and hydrogen peroxide inhibit *C. elegans* feeding
633 through gustatory receptor orthologs and pharyngeal neurons. Neuron *85*, 804-818.
634 Brockie, P.J., Madsen, D.M., Zheng, Y., Mellem, J., and Maricq, A.V. (2001). Differential
635 expression of glutamate receptor subunits in the nervous system of *Caenorhabditis*
636 *elegans* and their regulation by the homeodomain protein UNC-42. J. Neurosci. *21*,
637 1510-1522.
638 Burkewitz, K., Choe, K., and Strange, K. (2011). Hypertonic stress induces rapid and widespread
639 protein damage in *C. elegans*. Am J Physiol Cell Physiol *301*, C566-576.
640 Burkewitz, K., Choe, K.P., Lee, E.C., Deonarine, A., and Strange, K. (2012). Characterization of
641 the proteostasis roles of glycerol accumulation, protein degradation and protein
642 synthesis during osmotic stress in *C. elegans*. PLoS One *7*, e34153.
643 Chandler-Brown, D., Choi, H., Park, S., Ocampo, B.R., Chen, S., Le, A., Sutphin, G.L.,
644 Shamieh, L.S., Smith, E.D., and Kaeberlein, M. (2015). Sorbitol treatment extends
645 lifespan and induces the osmotic stress response in *Caenorhabditis elegans*. Front Genet
646 *6*, 316.
647 Choe, K.P. (2013). Physiological and molecular mechanisms of salt and water homeostasis in the
648 nematode *Caenorhabditis elegans*. Am J Physiol Regul Integr Comp Physiol *305*, R175-
649 186.
650 Choe, K.P., and Strange, K. (2007a). Evolutionarily conserved WNK and Ste20 kinases are
651 essential for acute volume recovery and survival after hypertonic shrinkage in
652 *Caenorhabditis elegans*. Am J Physiol Cell Physiol *293*, C915-927.
653 Choe, K.P., and Strange, K. (2007b). Molecular and genetic characterization of osmosensing and
654 signal transduction in the nematode *Caenorhabditis elegans*. FEBS J *274*, 5782-5789.

655 Choe, K.P., and Strange, K. (2008). Genome-wide RNAi screen and in vivo protein aggregation
656 reporters identify degradation of damaged proteins as an essential hypertonic stress
657 response. Am J Physiol Cell Physiol *295*, C1488-1498.
658 Cook, S.J., Crouse, C.M., Yemini, E., Hall, D.H., Emmons, S.W., and Hobert, O. (2020). The
659 connectome of the *Caenorhabditis elegans* pharynx. J Comp Neurol *528*, 2767-2784.
660 Cornell, R., Cao, W., Liu, J., and Pocock, R. (2022). Conditional degradation of UNC-31/CAPS
661 enables spatiotemporal analysis of neuropeptide function. J Neurosci *42*, 8599-8607.
662 Croset, V., Rytz, R., Cummins, S.F., Budd, A., Brawand, D., Kaessmann, H., Gibson, T.J., and
663 Benton, R. (2010). Ancient protostome origin of chemosensory ionotropic glutamate
664 receptors and the evolution of insect taste and olfaction. PLoS Genet *6*, e1001064.
665 Culotti, J.G., and Russell, R.L. (1978). Osmotic avoidance defective mutants of the nematode
666 *Caenorhabditis elegans*. Genetics *90*, 243-256.
667 Dobin, A., Davis, C.A., Schlesinger, F., Drenkow, J., Zaleski, C., Jha, S., Batut, P., Chaisson,
668 M., and Gingeras, T.R. (2013). STAR: ultrafast universal RNA-seq aligner.
669 Bioinformatics *29*, 15-21.
670 Dodd, W., Tang, L., Lone, J.C., Wimberly, K., Wu, C.W., Consalvo, C., Wright, J.E., Pujol, N.,
671 and Choe, K.P. (2018). A damage sensor associated with the cuticle coordinates three
672 core environmental stress responses in *Caenorhabditis elegans*. Genetics *208*, 1467-
673 1482.
674 Edgar, R.C. (2004). MUSCLE: a multiple sequence alignment method with reduced time and
675 space complexity. BMC Bioinformatics *5*, 113.
676 Etchberger, J.F., Lorch, A., Sleumer, M.C., Zapf, R., Jones, S.J., Marra, M.A., Holt, R.A.,
677 Moerman, D.G., and Hobert, O. (2007). The molecular signature and cis-regulatory
678 architecture of a *C. elegans* gustatory neuron. Genes Dev *21*, 1653-1674.
679 Eyun, S.I., Soh, H.Y., Posavi, M., Munro, J.B., Hughes, D.S.T., Murali, S.C., Qu, J., Dugan, S.,
680 Lee, S.L., Chao, H.*, et al.* (2017). Evolutionary history of chemosensory-related gene
681 families across the Arthropoda. Mol Biol Evol *34*, 1838-1862.
682 Ferkey, D.M., Sengupta, P., and L'Etoile, N.D. (2021). Chemosensory signal transduction in
683 *Caenorhabditis elegans*. Genetics *217*, iyab004.
684 Furness, J.B., Kunze, W.A., and Clerc, N. (1999). Nutrient tasting and signaling mechanisms in
685 the gut. II. The intestine as a sensory organ: neural, endocrine, and immune responses.
686 Am J Physiol *277*, G922-928.
687 Furness, J.B., and Stebbing, M.J. (2018). The first brain: Species comparisons and evolutionary
688 implications for the enteric and central nervous systems. Neurogastroenterol Motil *30*,
689 doi: 10.1111/nmo.13234. .
690 Graeve, A., Huster, J., Mayweg, F.R., Plassman, J., Wahle, P., and L.C., W. (2022). Functional
691 assessment of the ionotropic receptors IR25a and IR93a in predator perception in the
692 freshwater crustacean *Daphnia* using RNA interference. bioRxiv
693 https://doi.org/10.1101/2022.02.11.480022
694 Groh-Lunow, K.C., Getahun, M.N., Grosse-Wilde, E., and Hansson, B.S. (2014). Expression of
695 ionotropic receptors in terrestrial hermit crab's olfactory sensory neurons. Front Cell
696 Neurosci *8*, 448.
697 Hao, L., Johnsen, R., Lauter, G., Baillie, D., and Burglin, T.R. (2006). Comprehensive analysis
698 of gene expression patterns of hedgehog-related genes. BMC Genomics *7*, 280.
699 Hobert, O. (2013). The neuronal genome of *Caenorhabditis elegans*. WormBook, 1-106.

700 Huang, C.G., Lamitina, T., Agre, P., and Strange, K. (2007). Functional analysis of the
701 aquaporin gene family in *Caenorhabditis elegans*. Am J Physiol Cell Physiol *292*,
702 C1867-1873.
703 Huang, Y.C., Luo, J., Huang, W., Baker, C.M., Gomes, M.A., Meng, B., Byrne, A.B., and
704 Flavell, S.W. (2023). A single neuron in *C. elegans* orchestrates multiple motor outputs
705 through parallel modes of transmission. Curr Biol *33*, 4430-4445 e4436.
706 Hunter, R.W., Dhaun, N., and Bailey, M.A. (2022). The impact of excessive salt intake on
707 human health. Nat Rev Nephrol *18*, 321-335.
708 Igual Gil, C., Jarius, M., von Kries, J.P., and Rohlfing, A.K. (2017). Neuronal chemosensation
709 and osmotic stress response converge in the regulation of *aqp-8* in *C. elegans*. Front
710 Physiol *8*, 380.
711 Jacob, T.C., and Kaplan, J.M. (2003). The EGL-21 carboxypeptidase E facilitates acetylcholine
712 release at *Caenorhabditis elegans* neuromuscular junctions. J Neurosci *23*, 2122-2130.
713 Khan, M., Hartmann, A.H., O'Donnell, M.P., Piccione, M., Pandey, A., Chao, P.-H., Dwyer,
714 N.D., Bargmann, C.I., and Sengupta, P. (2022). Context-dependent reversal of odorant
715 preference is driven by inversion of the response in a single sensory neuron type. PLoS
716 Biol *20*, e3001677.
717 Kim, B., Hwang, G., Yoon, S.E., Kuang, M.C., Wang, J.W., Kim, Y.J., and Suh, G.S.B. (2024).
718 Postprandial sodium sensing by enteric neurons in *Drosophila*. Nat Metab *6*, 837-846.
719 Kim, K., and Li, C. (2004). Expression and regulation of an FMRFamide-related neuropeptide
720 gene family in *Caenorhabditis elegans*. J Comp Neurol *475*, 540-550.
721 Kinsman, B.J., Browning, K.N., and Stocker, S.D. (2017). NaCl and osmolarity produce
722 different responses in organum vasculosum of the lamina terminalis neurons,
723 sympathetic nerve activity and blood pressure. J Physiol *595*, 6187-6201.
724 Lamitina, S.T., Morrison, R., Moeckel, G.W., and Strange, K. (2004). Adaptation of the
725 nematode *Caenorhabditis elegans* to extreme osmotic stress. Am J Physiol Cell Physiol
726 *286*, C785-791.
727 Lamitina, S.T., and Strange, K. (2005). Transcriptional targets of DAF-16 insulin signaling
728 pathway protect *C. elegans* from extreme hypertonic stress. Am J Physiol Cell Physiol
729 *288*, C467-474.
730 Lamitina, T., Huang, C.G., and Strange, K. (2006). Genome-wide RNAi screening identifies
731 protein damage as a regulator of osmoprotective gene expression. Proc Natl Acad Sci
732 USA *103*, 12173-12178.
733 Lee, E.C., Kim, H., Ditano, J., Manion, D., King, B.L., and Strange, K. (2016). Abnormal
734 osmotic avoidance behavior in *C. elegans* is associated with increased hypertonic stress
735 resistance and improved proteostasis. PLoS One *11*, e0154156.
736 Love, M.I., Huber, W., and Anders, S. (2014). Moderated estimation of fold change and
737 dispersion for RNA-seq data with DESeq2. Genome Biol *15*, 550.
738 Miguel-Aliaga, I., Jasper, H., and Lemaitre, B. (2018). Anatomy and physiology of the digestive
739 tract of *Drosophila melanogaster*. Genetics *210*, 357-396.
740 Ni, L. (2020). The structure and function of Ionotropic Receptors in *Drosophila*. Front Mol
741 Neurosci *13*, 638839.
742 Nishimura, K., Fukagawa, T., Takisawa, H., Kakimoto, T., and Kanemaki, M. (2009). An auxin-
743 based degron system for the rapid depletion of proteins in nonplant cells. Nat Methods *6*,
744 917-922.

745 Policarpo, M., Baldwin, M.W., Casane, D., and Salzburger, W. (2024). Diversity and evolution
746 of the vertebrate chemoreceptor gene repertoire. Nat Commun *15*, 1421.
747 Possik, E., Schmitt, C., Al-Mass, A., Bai, Y., Cote, L., Morin, J., Erb, H., Oppong, A., Kahloan,
748 W., Parker, J.A.*, et al.* (2022). Phosphoglycolate phosphatase homologs act as glycerol-
749 3-phosphate phosphatase to control stress and healthspan in *C. elegans*. Nat Commun
750 *13*, 177.
751 Prescott, S.L., and Liberles, S.D. (2022). Internal senses of the vagus nerve. Neuron *110*, 579-
752 599.
753 Rhoades, J.L., Nelson, J.C., Nwabudike, I., Yu, S.K., McLachlan, I.G., Madan, G.K., Abebe, E.,
754 Powers, J.R., Colon-Ramos, D.A., and Flavell, S.W. (2019). ASICs mediate food
755 responses in an enteric serotonergic neuron that controls foraging behaviors. Cell *176*,
756 85-97 e14.
757 Rohlfing, A.K., Miteva, Y., Hannenhalli, S., and Lamitina, T. (2010). Genetic and physiological
758 activation of osmosensitive gene expression mimics transcriptional signatures of
759 pathogen infection in *C. elegans*. PLoS One *5*, e9010.
760 Rohlfing, A.K., Miteva, Y., Moronetti, L., He, L., and Lamitina, T. (2011). The *Caenorhabditis*
761 *elegans* mucin-like protein OSM-8 negatively regulates osmosensitive physiology via
762 the transmembrane protein PTR-23. PLoS Genet *7*, e1001267.
763 Rucker, A.J., Rudemiller, N.P., and Crowley, S.D. (2018). Salt, hypertension, and immunity.
764 Annu Rev Physiol *80*, 283-307.
765 Sanchez-Gracia, A., Vieira, F.G., and Rozas, J. (2009). Molecular evolution of the major
766 chemosensory gene families in insects. Heredity (Edinb) *103*, 208-216.
767 Sang, J., Dhakal, S., Shrestha, B., Nath, D.K., Kim, Y., Ganguly, A., Montell, C., and Lee, Y.
768 (2024). A single pair of pharyngeal neurons functions as a commander to reject high salt
769 in *Drosophila melanogaster*. eLife *12*, RP93464.
770 Serra, N.D., Darwin, C.B., and Sundaram, M.V. (2024). *Caenorhabditis elegans* Hedgehog-
771 related proteins are tissue- and substructure-specific components of the cuticle and
772 precuticle. Genetics *227*, iyae081.
773 Sieburth, D., Madison, J.M., and Kaplan, J.M. (2007). PKC-1 regulates secretion of
774 neuropeptides. Nat Neurosci *10*, 49-57.
775 Solomon, A., Bandhakavi, S., Jabbar, S., Shah, R., Beitel, G.J., and Morimoto, R.I. (2004).
776 *Caenorhabditis elegans* OSR-1 regulates behavioral and physiological responses to
777 hyperosmotic environments. Genetics *167*, 161-170.
778 Speese, S., Petrie, M., Schuske, K., Ailion, M., Ann, K., Iwasaki, K., Jorgensen, E.M., and
779 Martin, T.F. (2007). UNC-31 (CAPS) is required for dense-core vesicle but not synaptic
780 vesicle exocytosis in *Caenorhabditis elegans*. J Neurosci *27*, 6150-6162.
781 Spencer, N.J., and Hu, H. (2020). Enteric nervous system: sensory transduction, neural circuits
782 and gastrointestinal motility. Nat Rev Gastroenterol Hepatol *17*, 338-351.
783 Stocker, S.D., Kinsman, B.J., Farquhar, W.B., Gyarmati, G., Peti-Peterdi, J., and Sved, A.F.
784 (2024). Physiological mechanisms of dietary salt sensing in the brain, kidney, and
785 gastrointestinal tract. Hypertension *81*, 447-455.
786 Taruno, A., and Gordon, M.D. (2023). Molecular and cellular mechanisms of salt taste. Annu
787 Rev Physiol *85*, 25-45.
788 Taruno, A., Nomura, K., Kusakizako, T., Ma, Z., Nureki, O., and Foskett, J.K. (2021). Taste
789 transduction and channel synapses in taste buds. Pflugers Arch *473*, 3-13.

790 Taylor, S.R., Santpere, G., Weinreb, A., Barrett, A., Reilly, M.B., Xu, C., Varol, E., Oikonomou,
791 P., Glenwinkel, L., McWhirter, R.*, et al.* (2021). Molecular topography of an entire
792 nervous system. Cell *184*, 4329-4347 e4323.
793 Uchida, O., Nakano, H., Koga, M., and Ohshima, Y. (2003). The *C. elegans che-1* gene encodes
794 a zinc finger transcription factor required for specification of the ASE chemosensory
795 neurons. Development *130*, 1215-1224.
796 Urso, S.J., Comly, M., Hanover, J.A., and Lamitina, T. (2020). The O-GlcNAc transferase OGT
797 is a conserved and essential regulator of the cellular and organismal response to
798 hypertonic stress. PLoS Genet *16*, e1008821.
799 Urso, S.J., and Lamitina, T. (2021). The *C. elegans* hypertonic stress response: Big insights from
800 shrinking worms. Cell Physiol Biochem *55*, 89-105.
801 Valencia-Montoya, W.A., Pierce, N.E., and Bellono, N.W. (2024). Evolution of Sensory
802 Receptors. Annu Rev Cell Dev Biol *40*, 353-379.
803 van Giesen, L., and Garrity, P.A. (2017). More than meets the IR: the expanding roles of variant
804 Ionotropic Glutamate Receptors in sensing odor, taste, temperature and moisture.
805 F1000Res *6*, 1753.
806 Vidal, B., Gulez, B., Cao, W.X., Leyva-Diaz, E., Reilly, M.B., Tekieli, T., and Hobert, O.
807 (2022). The enteric nervous system of the *C. elegans* pharynx is specified by the Sine
808 oculis-like homeobox gene *ceh-34*. Elife *11*, e76003.
809 Watanabe, H., Fujisawa, T., and Holstein, T.W. (2009). Cnidarians and the evolutionary origin
810 of the nervous system. Dev Growth Differ *51*, 167-183.
811 Wheeler, J.M., and Thomas, J.H. (2006). Identification of a novel gene family involved in
812 osmotic stress response in *Caenorhabditis elegans*. Genetics *174*, 1327-1336.
813 Wimberly, K., and Choe, K.P. (2022). An extracellular matrix damage sensor signals through
814 membrane-associated kinase DRL-1 to mediate cytoprotective responses in
815 *Caenorhabditis elegans*. Genetics *220*, iyab217.
816 Zhang, L., Ward, J.D., Cheng, Z., and Dernburg, A.F. (2015). The auxin-inducible degradation
817 (AID) system enables versatile conditional protein depletion in *C. elegans*. Development
818 *142*, 4374-4384.
819

820
821

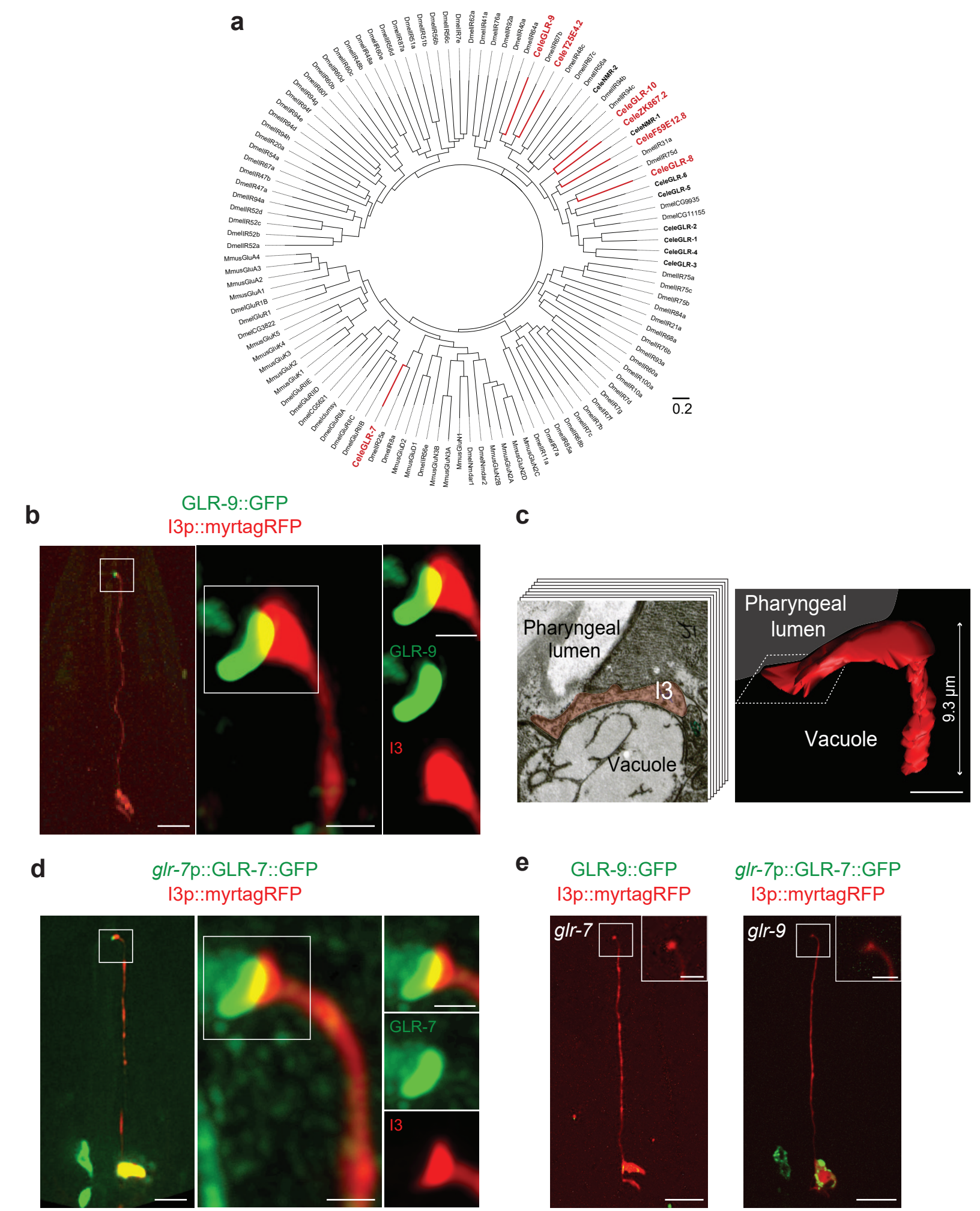

Yeon et al
Figure 1

822 **Fig. 1. GLR-9 and GLR-7 are localized at the pharyngeal lumen-exposed sensory ending of**
823 **I3.**
824 **a)** A rooted polar phylogenetic tree of ionotropic glutamate receptor sequences from *Drosophila*
825 (Dmel), *C. elegans* (Cele; bolded) and mouse (Mmus). Variant *C. elegans* IRs are indicated in
826 bold red; canonical ionotropic glutamate receptors are in bold black. The scale bar represents the
827 branch length, with each unit equivalent to 0.2 nucleotide substitutions per site.
828 **b,d)** Representative images of GLR-9 (b) or GLR-7 (d) fusion protein localization in I3. The I3
829 sensory ending is boxed and magnified in images on the right. GLR-9 is tagged with GFP at its
830 endogenous locus; *glr-7*p::GLR-7::GFP is expressed from an extrachromosomal array. I3 is
831 marked via the expression of *glr-9*p::myrtagRFP. Anterior is at top in all images. Scale bars: 10
832 μm (images at left); 0.5 μm (images at center and right).
833 **c)** (Left) Cross-section electron microscope image approximately 20 μm from the worm nose
834 showing the pharyngeal lumen, a vacuole, and I3 (shaded). (Right) 3D reconstruction of the I3
835 distal ending from electron microscope serial sections. The location of the pharyngeal lumen is
836 shown. The length of the reconstructed I3 ending is indicated at right. A dashed box indicates the
837 approximate position of the electron microscope cross-section image shown at left. Arrowhead
838 indicates the sensory ending. Scale bar: 0.25 μm.
839 **e)** Localization of GLR-9::GFP or GLR-7::GFP in I3 in *glr-7(tm2877)* or *glr-9(oy180)* mutant
840 backgrounds, respectively. Anterior is at top. The I3 sensory ending is boxed and magnified in
841 the insets. Scale bars: 10 μm; 2.5 μm (insets).
842

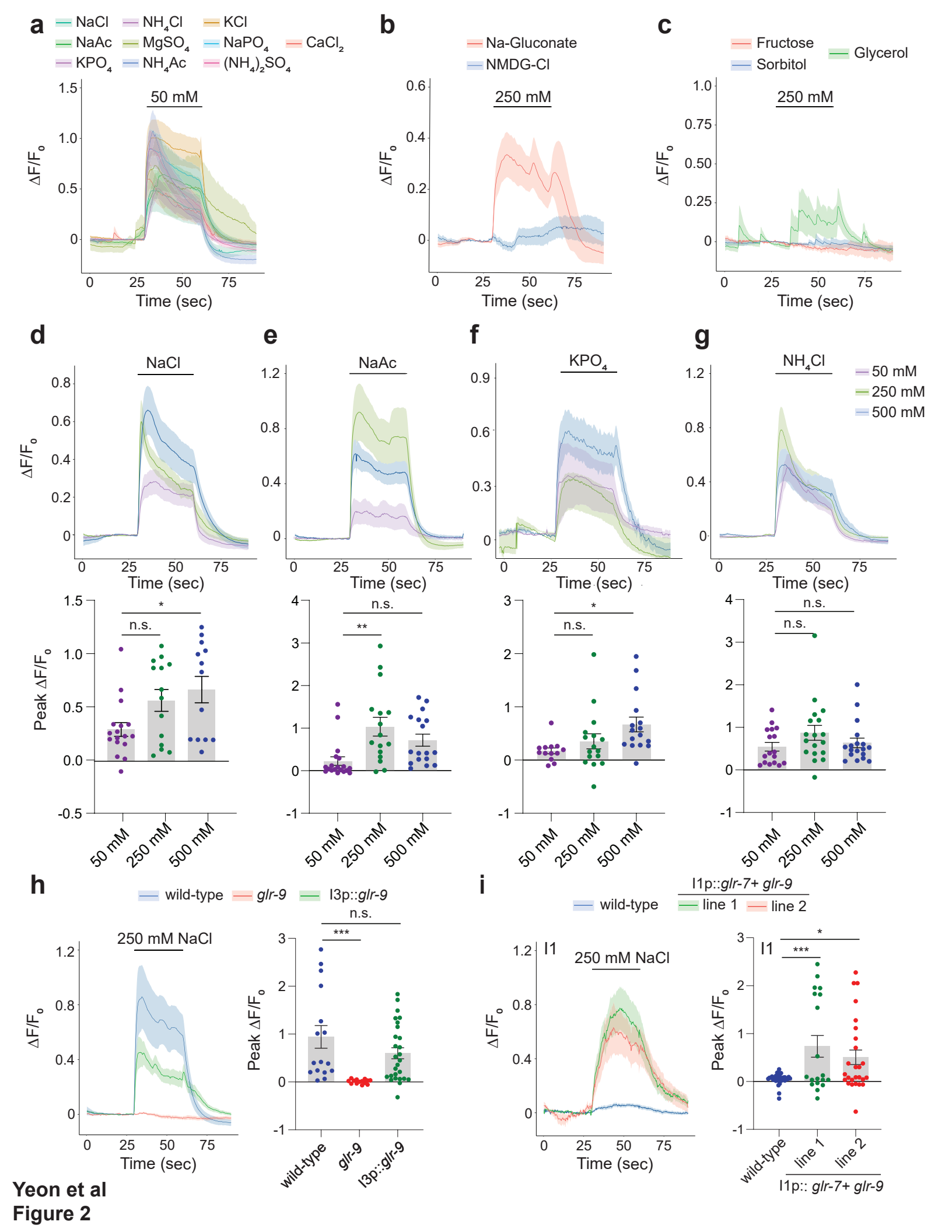

Yeon et al
Figure 2

843 **Fig. 2. I3 responds to multiple monovalent and divalent cations in a GLR-9-dependent**
844 **manner.**
845 **a-c)** Average changes in GCaMP6s fluorescence in I3 in response to a 30 sec pulse of the
846 indicated salts (a,b) or sugars (c) at the shown concentrations. Quantification of peak
847 fluorescence intensities are shown in Fig. S2b-d.
848 **d-g)** Average (top) and peak intensity changes (bottom) of GCaMP6s fluorescence in I3 in
849 response to a 30 sec pulse of different concentrations of NaCl, NaAc, KPO_4, and NH_4Cl. * and
850 ** indicate different from corresponding 50 mM values at P< 0.05 and 0.01, respectively (one-
851 way ANOVA and Dunnett's test).
852 **h)** Average (left) and peak intensity changes (right) of GCaMP6s fluorescence in I3 in response
853 to a 30 sec pulse of 250 mM NaCl in animals of the indicated genotypes. The *glr-9(oy180)* allele
854 was used. Wild-type *glr-9* sequences were expressed in I3 under the *glr-9* promoter. Rescue data
855 shown are combined values from two independent transgenic lines; responses of each line were
856 similar. *** indicates different from wild-type at P<0.001 (one-way ANOVA and Dunnett's
857 test).
858 **i)** Average (left) and peak intensity changes (right) of GCaMP6s fluorescence in wild-type I1
859 neurons or in I1 misexpressing GLR-7 and GLR-9 to a 30 sec pulse of 250 mM NaCl.
860 Expression in I1 was driven under the *lgc-8* promoter. Responses from two independent
861 misexpressing lines are shown. * and *** indicate different from wild-type I1 at P<0.01 and
862 0.001, respectively (one-way ANOVA and Dunnett's test).
863 Shaded regions in all traces indicate SEM. Each dot in the scatter plots is the value from a single
864 neuron. Horizontal lines in scatter plots indicate the mean; errors are SEM. Data shown are from
865 2-3 independent experiments each. n.s. – not significant.

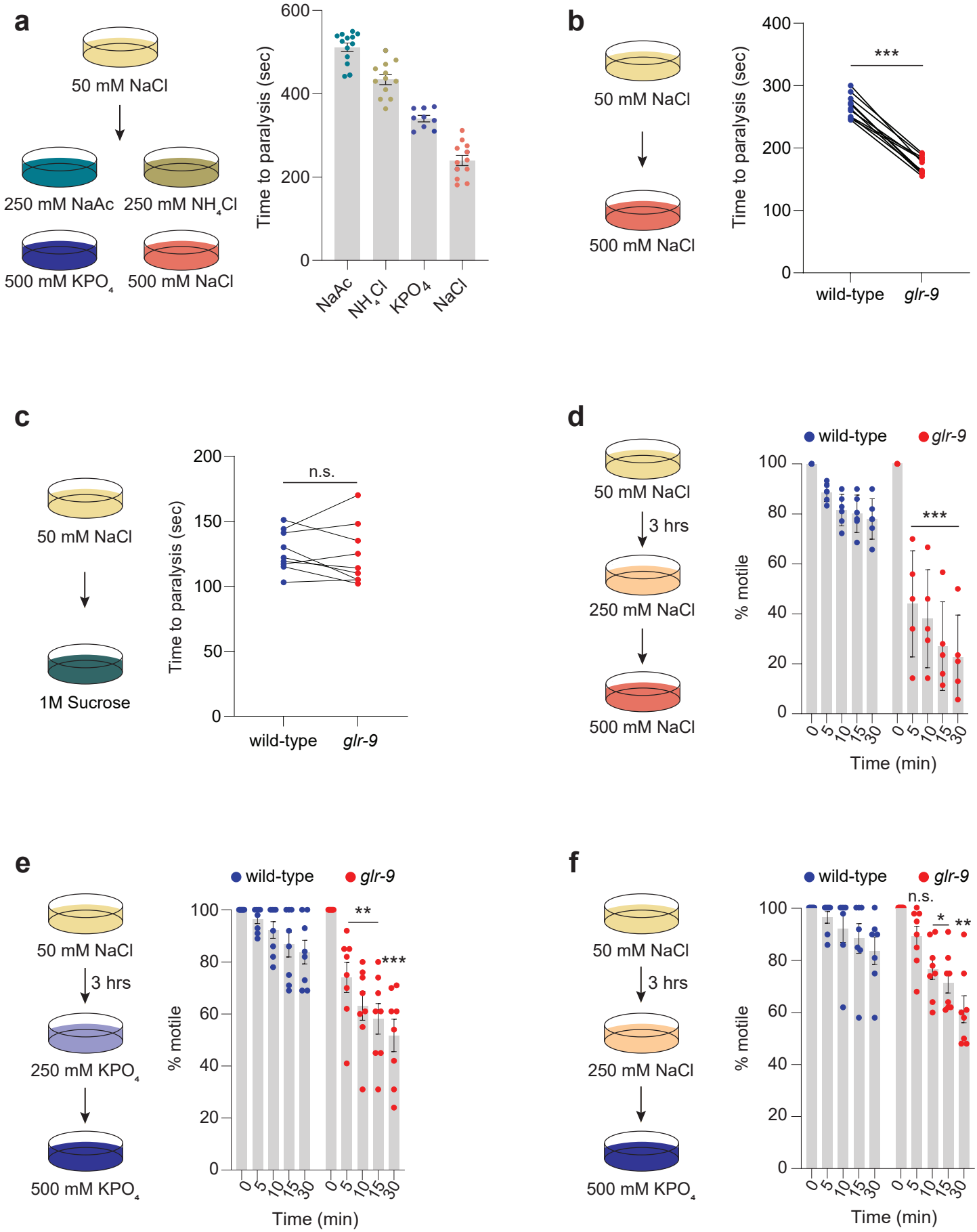

Yeon et al
Figure 3

866 **Fig. 3. *glr-9* mutants exhibit reduced tolerance of high salt.**

867 **a)** (Left) Cartoon of experimental conditions. (Right) Quantification of time to paralysis upon
868 shifting animals to each salt at concentrations indicated in the cartoon. Each dot is the time at
869 which all ten animals in a single assay are immotile following the shift to high salt.

870 **b,c)** Quantification of time to paralysis upon shifting animals of the indicated genotypes from 50
871 to 500 mM NaCl or equiosmolar 1 M sucrose (cartoon at left). Each dot is the time at which all
872 ten animals in a single assay are immotile. Wild-type and *glr-9* mutants were examined in
873 parallel in the same assay. *** indicates different from wild-type at P<0.001 (t-test).

874 **d-f)** Percentage of animals of the indicated genotypes that are motile at each time point following
875 a shift from the acclimation plate (250 mM salt for 3 hrs) to 500 mM salt (cartoons at left). Each
876 dot is the value from a single assay; n=30 animals per assay. *, **, and *** indicate different
877 from wild-type at the corresponding time at P<0.05, 0.01, and 0.001 (one-day ANOVA and
878 Dunnett's test).

879 The *glr-9(oy180)* allele was used in all experiments. Horizontal lines in scatter plots indicate the
880 mean; errors are SEM. Data shown are from 2-3 independent experiments each. n.s. – not
881 significant.

882

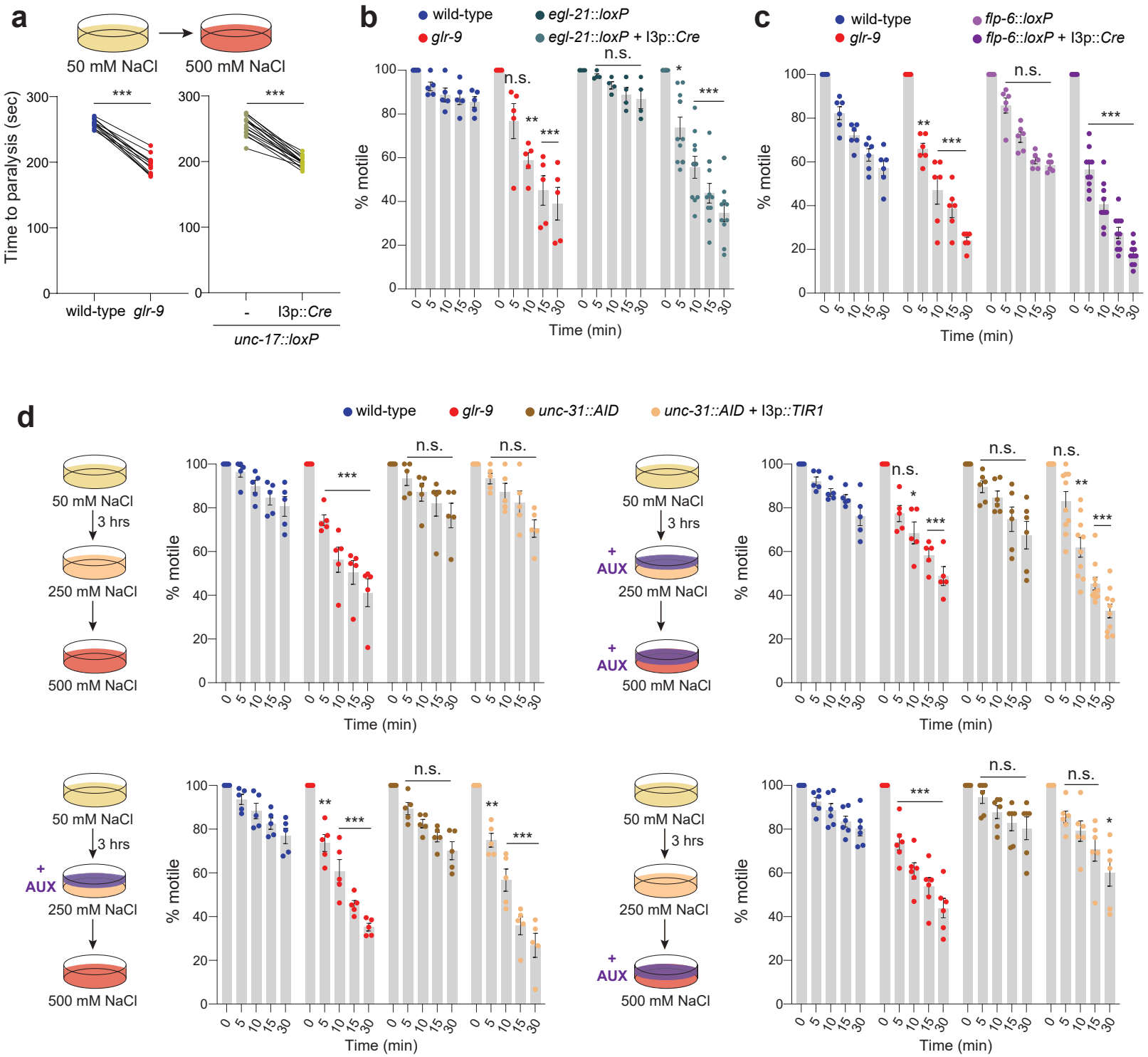

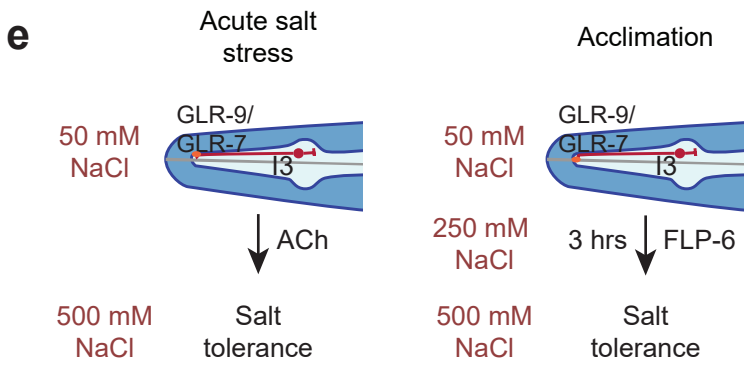

Yeon et al
Figure 4

883 **Fig. 4. Cholinergic and FLP-6-mediated peptidergic signaling from I3 are necessary for**
884 **high salt tolerance in unacclimated and acclimated animals, respectively.**
885 **a)** Quantification of time to paralysis upon shifting animals of the indicated genotypes from 50 to
886 500 mM NaCl (cartoon at top). Each dot is the time at which all ten animals in a single assay are
887 immotile. Cre was expressed in I3 under the *glr-9* promoter. Control and mutant animals were
888 examined in parallel in the same assay. *** indicates different from wild-type at P<0.001 (t-test).
889 **b,c)** Percentage of animals of the indicated genotypes that are motile at each time point following
890 a shift from the acclimation plate (250 mM NaCl for 3 hrs) to 500 mM NaCl. Each dot is the
891 value from a single assay; n=30 animals per assay. Cre was expressed in I3 under the *glr-9*
892 promoter. *, **, and *** indicate different from wild-type at the corresponding time at P<0.05,
893 0.01, and 0.001 (one-way ANOVA and Dunnett's test).
894 **d)** (Left in all panels) Cartoon of the experimental protocol. (Right in all panels) Percentage of
895 animals of the indicated genotypes that are motile at each time point following a shift from the
896 acclimation plate to the assay plate in the presence or absence of added exogenous auxin as
897 shown. TIR1 was expressed in I3 under the *glr-9* promoter. Each dot is the value from a single
898 assay; n=30 animals per assay. *, **, and *** indicate different from wild-type at the
899 corresponding time at P<0.05, 0.01, and 0.001 (one-way ANOVA and Dunnett's test).
900 **e)** Cholinergic signaling from I3 promotes high salt tolerance under conditions of acute salt
901 stress, whereas FLP-6 signaling from I3 during acclimation enables tolerance upon subsequent
902 exposure to high salt.
903 The *glr-9(oy180)* allele was used in all experiments. Horizontal lines in scatter plots indicate the
904 mean; errors are SEM. Data shown are from 2-3 independent experiments each. n.s-- not
905 significant.

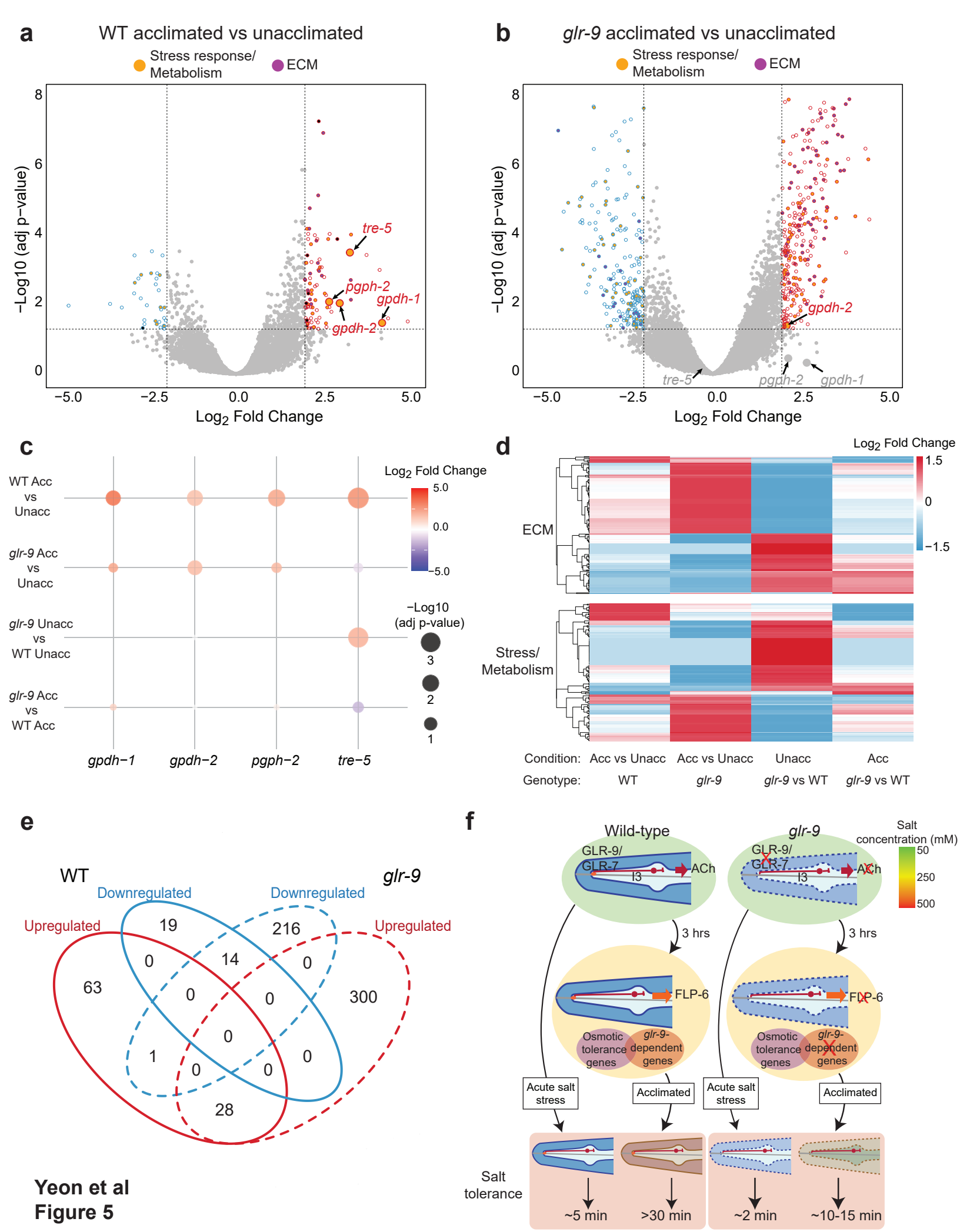

Yeon et al
Figure 5

906 **Fig. 5. GLR-9-mediated signaling is required for altered expression of a subset of**
907 **osmotolerance genes.**
908 **a,b)** Volcano plots of differential gene expression in unacclimated (50 mM NaCl) and salt
909 acclimated (250 mM NaCl for 3 hrs) wild-type and *glr-9(oy180)* animals. Horizontal and vertical
910 dashed lines indicate significant at adjusted p-value <0.05 and $\log_2$ fold change >2 or <−2,
911 respectively. A subset of osmolyte biosynthetic enzymes previously implicated in osmotolerance
912 is indicated. Differentially expressed genes predicted to encode molecules involved in stress
913 responses or metabolism, and cuticular components, are indicated in yellow and purple,
914 respectively.
915 **c)** Dot plot of average expression changes of the indicated genes in the shown genetic
916 backgrounds and conditions. Color indicates $\log_2$ fold change and size indicates adjusted p-value.
917 Blank indicates no expression change detected.
918 **d)** Hierarchically clustered heatmaps of differentially expressed genes categorized as being
919 involved in extracellular matrix remodeling (top) or in stress and metabolic responses (bottom)
920 in the indicated conditions and genetic backgrounds.
921 **e)** Venn diagram indicating unique and common differentially expressed genes in unacclimated
922 and acclimated wild-type and *glr-9(oy180)* mutants.
923 **f)** Working model of the contribution of GLR-9-mediated signaling to high salt tolerance. In the
924 absence of *glr-9* or cholinergic signaling from I3, remodeling of the cuticle even under isotonic
925 conditions may contribute to decreased resistance to acute high salt stress. Upon acclimation,
926 both GLR-9-dependent and -independent pathways contribute to cuticular remodeling and
927 altered expression of osmotolerance genes, thereby enabling prolonged tolerance of high salt.
928 The failure to alter expression of a subset of osmotolerance genes in *glr-9* mutants or upon loss

929 of FLP-6 signaling from I3, and/or the dysregulated gene expression program under isotonic and

930 acclimated conditions, reduces high salt tolerance following acclimation.

Movie S1. (Right) 3D-rendered image of GLR-9::GFP localization at the I3 sensory ending (Left) generated using Imaris Analysis Software (version 10.2.0).

Movie S2. 3D reconstruction of the I3 sensory ending from electron microscope serial sections.

Data Table 1. List of upregulated and downregulated genes and gene categories across each condition/genotype from RNA-Seq analysis. The category list is ordered from highest to lowest gene count.

Table S1. List of strains used in this work.

Strain name	Genotype	Source/ Parent strain
PY12290	*glr-9::gfp*(*sy5669*); *oyEx761* [*glr-9*p::*myr-TagRfp*; *unc-122*p::*dsRed*]	Suny Biotech, This paper
PY12291	*oyEx762* [*glr-7*p::*glr-7*::*gfp*; *glr-9*p:: *myr-TagRfp; unc-122*p::*dsRed*]	This paper
PY12292	*glr-7(tm2877)*; *glr-9::gfp*(*sy5669*); *oyEx761* [*glr-9*p::*myr-TagRfp*; *unc-122*p::*dsRed*]	CGC, This paper
PY12293	*glr-9*(*oy180*); *oyEx762* [*glr-7*p::*glr-7*::*gfp*; *glr-9*p:: *myr-TagRfp; unc-122*p::*dsRed*]	This paper
PY12286	*oyIs98* [*glr-9*p::GCaMP6s; *unc-122*p::*dsRed*]	This paper
PY12294	*glr-9*(*oy180*); *oyIs98* [*glr-9*p::GCaMP6s; *unc-122*p::*dsRed*]	This paper
PY12295	*glr-9*(*oy180*); *oyIs98* [*glr-9*p::GCaMP6s; *unc-122*p::*dsRed*]; *oyEx763* [*glr-9*p::*glr-9*::*TagRfp*; *unc-122*p::*gfp*] Line-1	This paper
PY12296	*glr-9*(*oy180*); *oyIs98* [*glr-9*p::GCaMP6s; *unc-122*p::*dsRed*]; *oyEx764* [*glr-9*p::*glr-9*::*TagRfp*; *unc-122*p::*gfp*] Line-2	This paper
PY12297	*unc-119*(*ed3*); *otIs898* [*pha-4*prom2::3xNLS::GCaMP6s::*unc-54* 3' UTR]; *oyEx765* [*lgc-8*p::*mCherry*; *unc-122*p::*dsRed*]	OH18562, This paper
PY12298	*unc-119*(*ed3*); *otIs898* [*pha-4*prom2::3xNLS::GCaMP6s::*unc-54* 3' UTR]; *oyEx765* [*lgc-5*p::*mCherry*; *unc-122*p::*dsRed*]; *oyEx766* [*lgc*-8p::*glr-7*::*TagRfp*; *lgc*-8p::*glr-9*::*TagRfp*; *unc-122*p::*gfp*] Line-1	OH18562, This paper
PY12299	*unc-119*(*ed3*); *otIs898*[*pha-4*prom2::3xNLS::GCaMP6s::*unc-54* 3' UTR]; *oyEx765* [*lgc-5*p::*mCherry*; *unc-122*p::*dsRed*]; *oyEx767* [*lgc*-8p::*glr-7*::*TagRfp*; *lgc*-8p::*glr-9*::*TagRfp*; *unc-122*p:: *gfp*] Line-2	OH18562, This paper
PY12230	*glr-9*(*oy180*)	This paper
PY12228	*oyEx717* [*glr-9*p::*Chrimson::*T2A*::mCherry*; *unc-122*p::*gfp*] Line-1	This paper
PY12289	*glr-9*(*oy180*); *oyEx717* [*glr-9*p::*Chrimson::*T2A*::mCherry*; *unc-122*p::*gfp*]	This paper
PY12800	*loxP*::*unc-17*::*loxP* (*syb5779 syb5987*)	SWF1012, This paper
PY12801	*loxP*::*unc-17*::*loxP* (*syb5779 syb5987*); *oyEx768* [*glr-9*p::*Cre*::SL2::*gfp*; *unc-122*p::*gfp*]	SWF1012, This paper
PY12802	*egl-21*(*n476*); *kySi61* [*loxP::egl-21genomic::loxP*]	SWF717, This paper

PY12803	*egl-21*(*n476*); *kySi61* [*loxP::egl-21genomic::loxP*]; *oyEx768* [*glr*-9p::*Cre*::SL2::*gfp*; *unc-122*p::*gfp*]	SWF717, This paper
VC2324	*flp-6*(*ok3056*)	CGC
PY12804	*glr-9(oy180)*; *flp-6*(*ok3056)*	This paper
PY12288	*loxP::flp-6::loxP*(*oy203)*	This paper
PY12805	*loxP::flp-6*::*loxP*(*oy203); oyEx768* [*glr*-9p::*Cre*::SL2::*gfp*; *unc-122*p::*gfp*]	This paper
RJP5269	*unc-31* (*rp166*[GFP::TEV::AID::FLAG::*unc-31*])	CGC
PY12806	*unc-31* (*rp166*[GFP::TEV::AID::FLAG::*unc-31*]); *oyEx769* [*glr-9*p::TIR1::*mScarlet*; *unc-122*p::*gfp*] Line-1	This paper
PY12807	*unc-31* (*rp166*[GFP::TEV::AID::FLAG::*unc-31 oyEx769* [*glr-9*p::TIR1::SL2::*mScarlet*; *unc-122*p::*gfp*] Line-2	This paper
PY12808	*unc-13(e51); oyIs98* [*glr-9*p::GCaMP6s; *unc-122*p::*dsRed*]	This paper
PY12809	*unc-31(e169); oyIs98* [*glr-9*p::GCaMP6s; *unc-122*p::*dsRed*]	This paper
PY12810	*tax-4*(*p678*); *oyIs98* [*glr-9*p::GCaMP6s; *unc-122*p::*dsRed*]	This paper
PY12811	*osm-9*(*oy202*); *oyIs98* [*glr-9*p::GCaMP6s; *unc-122*p::*dsRed*]	This paper
PY12812	*che-1*(*p674*); *oyIs98* [*glr-9*p::GCaMP6s; *unc-122*p::*dsRed*]	This paper
PY12813	*oyIs97* [*flp-6*p::GCaMP; *unc-122*p::*gfp*]; *oyEx770* [*che-1*p::*glr-9*::*TagRfp; che-1*p::*glr-7*::*TagRfp*; *unc-122*p::*dsRed*]	This paper
PR678	*tax-4*(*p678*)	CGC
CX10	*osm-9*(*ky10)*	CGC
CX4544	*ocr-2*(*ak47*)	CGC
FX30280	*flp-5*(*tm10075*)	NBRP
FX02427	*flp-13*(*tm2427*)	NBRP
AX1410	*flp-18*(*db99*)	CGC
FX02179	*flp-18*(*tm2179*)	NBRP
RB2269	*flp-34*(*ok3071*)	CGC
FX03023	*nlp-3*(*tm3023*)	NBRP
TM2569	*nlp-7*(*tm2984*)	NBRP
FX06232	*nlp-10*(*tm6232*)	NBRP
PHX530	*nlp-11*(*syb530*)	CGC
FX02569	*nlp-21*(*tm2569*)	NBRP
PS8789	*dmsr-1*(*sy1522*)	CGC
PS8854	*dmsr-7*(*sy1539*)	CGC
PS8483	*frpr-8*(*sy1362*)	CGC
MT14666	*egl-6*(*n4537*)	CGC

12

13 **Table S2.** List of plasmids used in this work.

Plasmid name	Description	Source
PSAB1374	*glr-9*p::*myr-TagRfp*	This paper
PSAB1373	*glr-7*p::*glr-7*::*gfp*	This paper
PSAB1383	*glr-9*p::GCaMP6s	This paper
PSAB1375	*glr-9*p::*glr-9*::*TagRfp*	This paper
PSAB1376	*lgc-8*p::*mCherry*	This paper
PSAB1378	*lgc*-8p::*glr-7*::*TagRfp*	This paper
PSAB1377	*lgc*-8p::*glr*-9::*TagRfp*	This paper
PSAB1371	*glr-9p::Chrimson::T2A::mCherry*	This paper
PSAB1379	*glr*-9p::*Cre*::*SL2*::*gfp*	This paper
PSAB1380	*glr-9*p::TIR1::*mScarlet*	This paper
PSAB1381	*che-1*p::*glr-7*::*TagRfp*	This paper
PSAB1382	*che-1*p::*glr-9*::*TagRfp*	This paper

14
15

REFERENCES

Albrecht, D.R., and Bargmann, C.I. (2011). High-content behavioral analysis of *Caenorhabditis elegans* in precise spatiotemporal chemical environments. Nat Methods *8*, 599-605.

Benton, R., Vannice, K.S., Gomez-Diaz, C., and Vosshall, L.B. (2009). Variant ionotropic glutamate receptors as chemosensory receptors in *Drosophila*. Cell *136*, 149-162.

Dodd, W., Tang, L., Lone, J.C., Wimberly, K., Wu, C.W., Consalvo, C., Wright, J.E., Pujol, N., and Choe, K.P. (2018). A damage sensor associated with the cuticle coordinates three core environmental stress responses in *Caenorhabditis elegans*. Genetics *208*, 1467-1482.

Khan, M., Hartmann, A.H., O'Donnell, M.P., Piccione, M., Pandey, A., Chao, P.-H., Dwyer, N.D., Bargmann, C.I., and Sengupta, P. (2022). Context-dependent reversal of odorant preference is driven by inversion of the response in a single sensory neuron type. PLoS Biol *20*, e3001677.

Rohlfing, A.K., Miteva, Y., Moronetti, L., He, L., and Lamitina, T. (2011). The *Caenorhabditis elegans* mucin-like protein OSM-8 negatively regulates osmosensitive physiology via the transmembrane protein PTR-23. PLoS Genet *7*, e1001267.

Taylor, S.R., Santpere, G., Weinreb, A., Barrett, A., Reilly, M.B., Xu, C., Varol, E., Oikonomou, P., Glenwinkel, L., McWhirter, R.*, et al.* (2021). Molecular topography of an entire nervous system. Cell *184*, 4329-4347 e4323.

Zheng, Y., Brockie, P.J., Mellem, J.E., Madsen, D.M., and Maricq, A.V. (1999). Neuronal control of locomotion in *C. elegans* is modified by a dominant mutation in the GLR-1 ionotropic glutamate receptor. Neuron *24*, 347-361.

Zuo, J., De Jager, P.L., Takahashi, K.A., Jiang, W., Linden, D.J., and Heintz, N. (1997). Neurodegeneration in Lurcher mice caused by mutation in delta2 glutamate receptor gene. Nature *388*, 769-773.

a

IR-like protein	TM #	Extended amino-terminal domain	Ala in TMIII	Arg in S1 domain	Thr in S2 domain	Asp or Glu in S2 domain
GLR-7	3	Yes	Yes	Yes	No	Yes
GLR-8	3	No	Yes	Yes	No	No
GLR-9	3	No	No	Yes	No	Yes
GLR-10	3	No	No	Yes	No	No
ZK867.2	3	No	Yes	Yes	No	No
F59E12.8	3	No	No	Yes	No	No
T25E4.2	3	No	No	Yes	No	No

b

IR-like gene	Expression In:	
	Pharyngeal Enteric Neurons	Somatic Neurons
glr-7	I3, I6, M3, NSM	PLM, ALM, PVM
glr-8	I6, NSM, I1, MI, MC, M3, I3, M5, I2	PVD, PHB, PHA, IL2, AVL, URB, PLM, ALM, ADL, AVM
glr-9	I3	none
glr-10	I6, NSM	none
ZK867.2	I6, NSM	PQR, PHA, PVD, AQR, ADL, AUA, AVH, URY, PHC, ASK, PHB, OLQ, URX, AVF, PVT, RIH
F59E12.8	none	none
T25E4.2	NSM, I6, MI	none

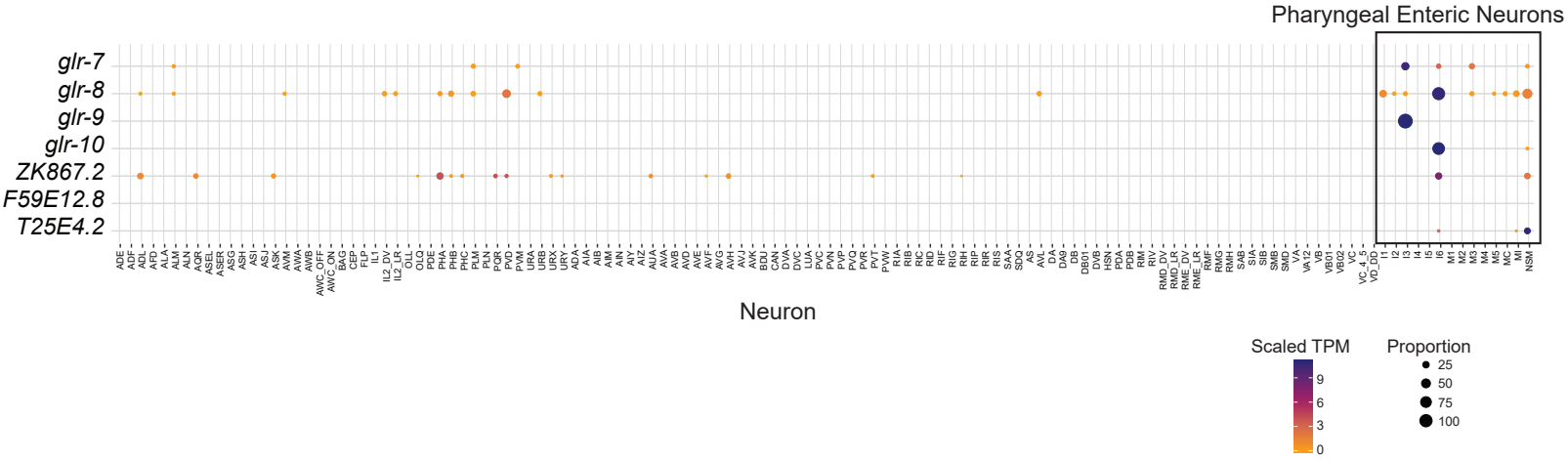

Yeon et al
Figure S1

43 **Fig. S1. *C. elegans* IR-like genes are expressed highly or exclusively in PENs.**

44 **a)** Features of IR-like proteins in *C. elegans*. TM: transmembrane domain. Mutating the

45 conserved Ala in TMIII in ionotropic glutamate receptors results in a constitutively open channel

46 (Zheng et al., 1999; Zuo et al., 1997). The Arg, and Thr and Asp/Glu residues, in the S1 and S2

47 ligand-binding domains, respectively, directly interact with glutamate or synthesized agonists in

48 ionotropic glutamate receptors (Benton et al., 2009).

49 **b)** Predicted expression of IR-like genes adapted from the *C. elegans* neuronal gene expression

50 map and network (CeNGEN) (Taylor et al., 2021).

51

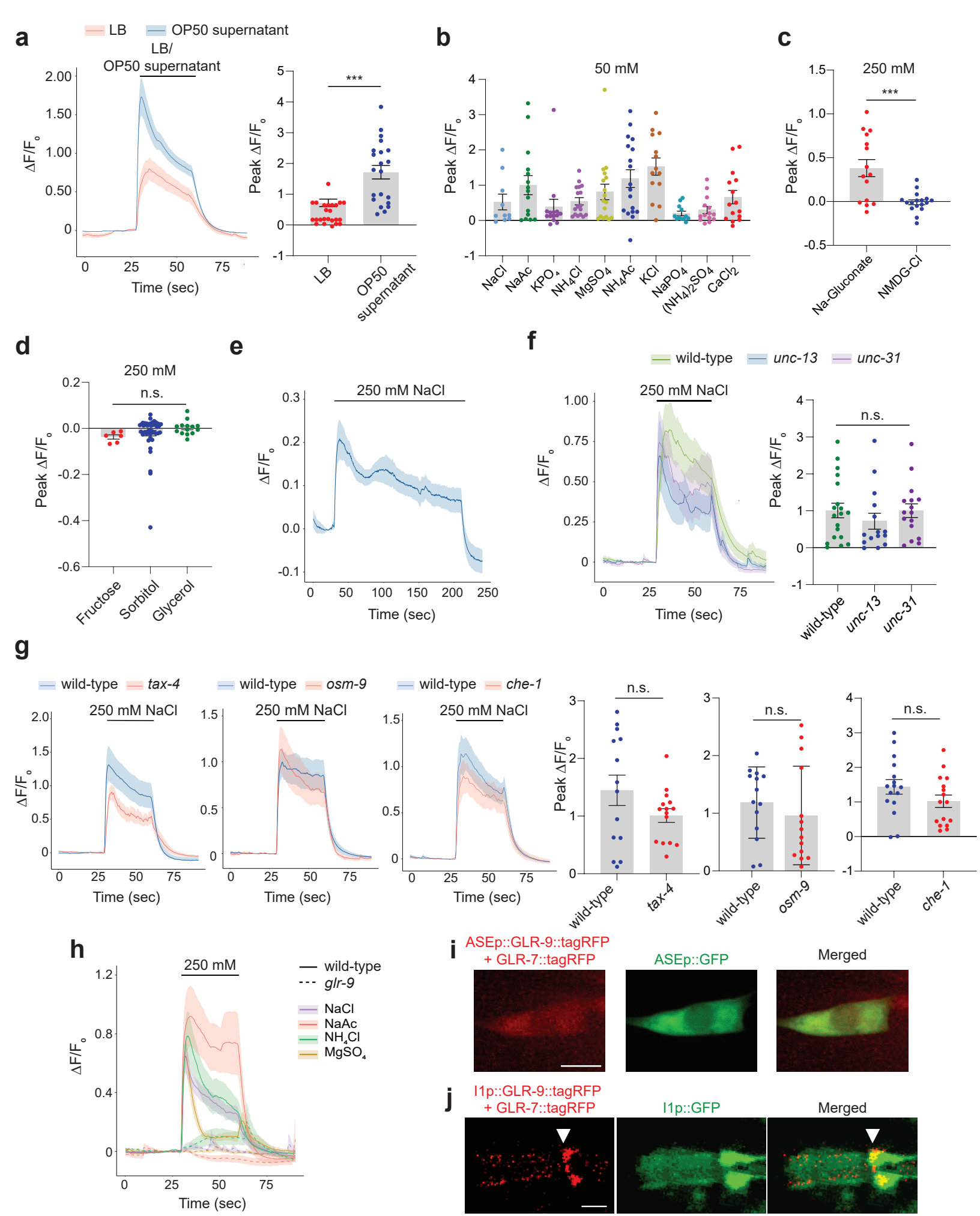

Yeon et al
Figure S2

52 **Fig. S2. I3 responds cell-autonomously to multiple cations via GLR-9.**

53 **a)** Average (left) and peak intensity changes (right) of GCaMP6s fluorescence in wild-type I3
54 neurons in response to a 30 sec pulse of LB alone or supernatant of an OP50 bacterial culture
55 grown in LB. *** indicates different at P<0.001 (t-test).

56 **b-d)** Peak fluorescence intensity changes in I3 in response to the indicated chemical
57 concentrations. Average traces are shown in Fig. 2a-c. *** indicates different at P<0.001 (c: t-
58 test; d: one-way ANOVA and Dunnett's test).

59 **e)** Mean GCaMP6s fluorescence change in I3 in response to a 3 min pulse of 250 mM NaCl.

60 **f,g)** Average (left) and peak intensity changes (right) of GCaMP6s fluorescence in I3 in response
61 to a 30 sec pulse of 250 mM NaCl in animals of the indicated genotypes. Alleles used were *unc-*
62 *13(e51), unc-31(e169)*, *tax-4(p678), osm-9(oy202),* and *che-1(p674).*

63 **h)** Mean GCaMP6s fluorescence changes in response to a 30 sec pulse of the indicated salts at
64 250 mM in wild-type and *glr-9(oy180)* mutants. n>17 each. Wild-type data were interleaved
65 with data in Fig. 2d-g, and are repeated.

66 **i,j)** Representative images of GLR-9/GLR-7::tagRFP localization in ASE soma (i), and I1 (j).
67 Expression in ASE and I1 was driven under the *che-1* and *lgc-8* promoters, respectively.
68 Arrowhead indicates the non-ciliated sensory ending of I1 in j. Anterior is at left in all images.
69 Scale bar: 5 μm.

70 Shaded regions in all traces indicate SEM. Each dot in the scatter plots is the value from a single
71 neuron. Horizontal lines in scatter plots indicate the mean; errors are SEM. Data shown are from
72 2-3 independent experiments each. n.s.- not significant.

73

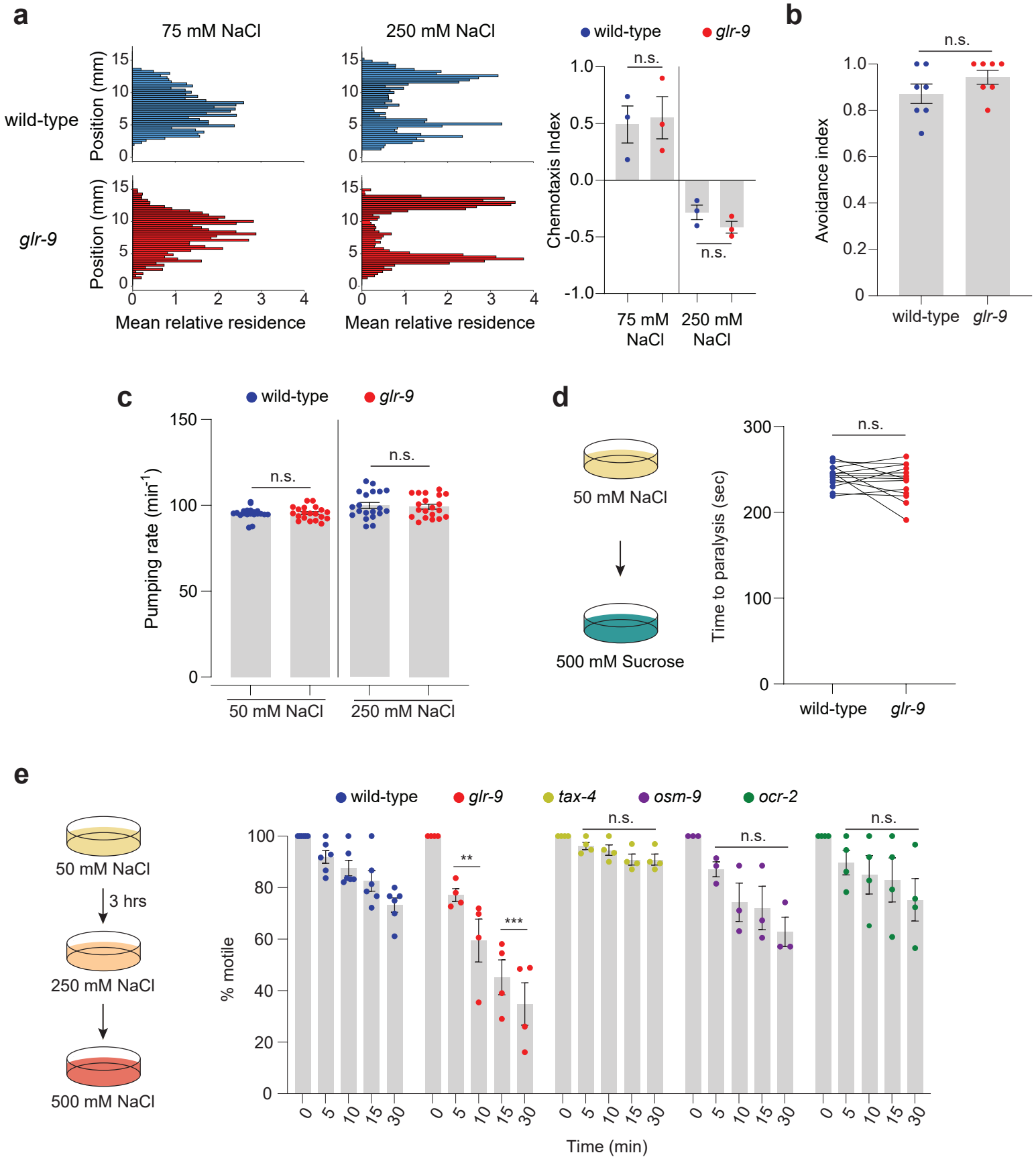

Yeon et al
Figure S3

74 **Fig. S3. *glr-9* mutants do not exhibit altered behavioral responses to salt.**

75 **a)** (Left) Histograms showing average relative residence of wild-type and *glr-9(oy180)* animals
76 in a microfluidics behavioral arena (Albrecht and Bargmann, 2011; Khan et al., 2022) with a
77 central stripe of the indicated salt concentrations. (Right) Chemotaxis indices quantified from the
78 microfluidics behavioral assays. Each dot is the index from a single assay of ~15 animals each.

79 **b)** Percentage of animals of the indicated genotypes remaining within the glycerol ring after 10
80 mins. Each dot is the value from a single assay of 10 animals each.

81 **c)** Pumping rate on bacteria-seeded plates containing the indicated salt concentrations. Each dot
82 is the measurement from a single animal.

83 **d)** Quantification of time to paralysis of wild-type or *glr-9* mutants in the shown assay conditions
84 (cartoons at left). Each dot is the time at which all ten animals in a single assay are immotile.
85 Wild-type and *glr-9* mutants were examined in parallel in the same assay.

86 **e)** Percentage of animals of the indicated genotypes that are motile at each time point following a
87 shift from the acclimation plate to the assay plate. Alleles used were *glr-9(oy180), tax-4(p678),*
88 *osm-9(ky10)*, and *ocr-2(ak47)*. Each dot is the value from a single assay; n=30 animals per assay.
89 ** and *** indicate different from wild-type at the corresponding time at $P<0.01$ and 0.001,
90 respectively (one-way ANOVA and Dunnett's test).

91 Horizontal lines in all scatter plots indicate the mean; errors are SEM. n.s. – not significant.

92

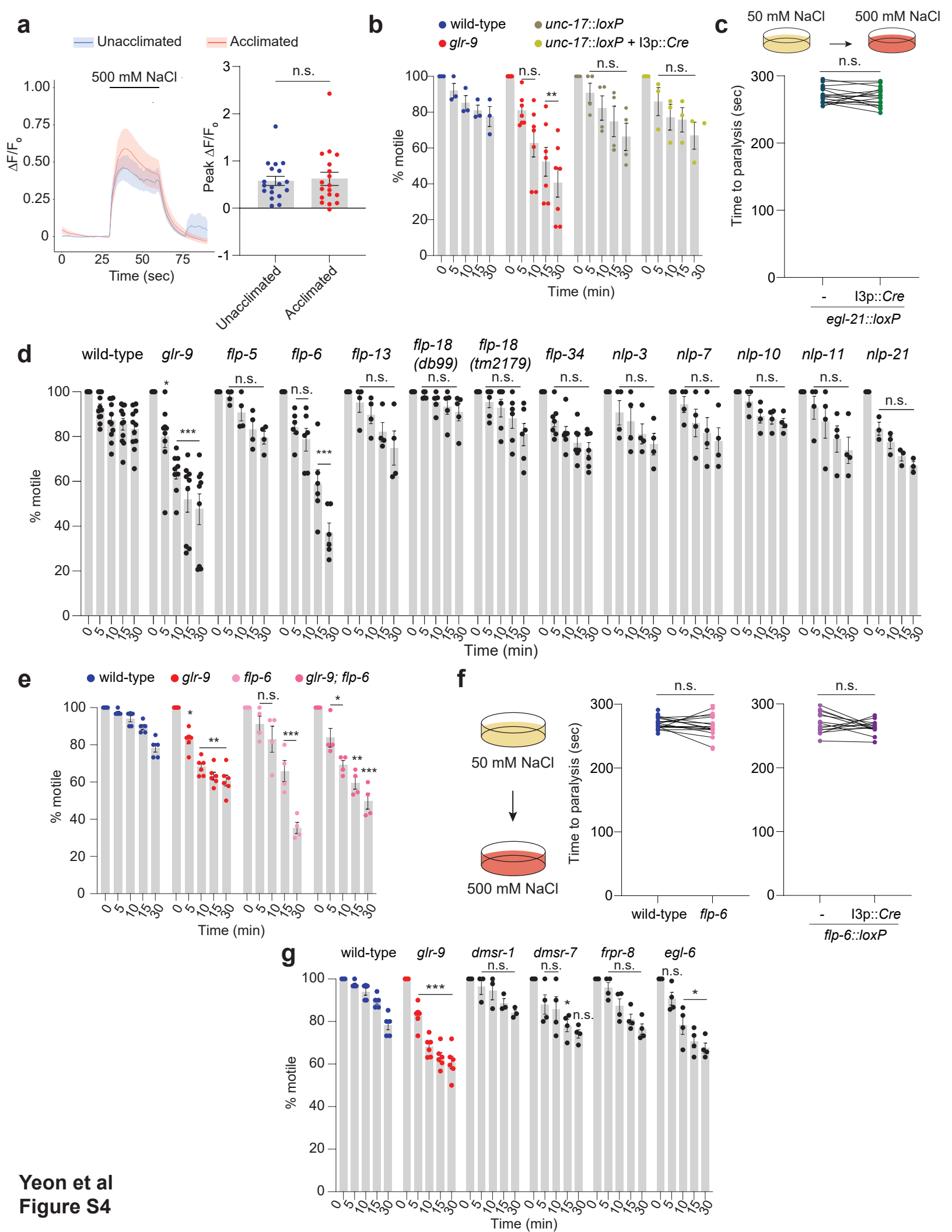

Yeon et al
Figure S4

93 **Fig. S4. Peptidergic but not cholinergic signaling from I3 is required for salt acclimation.**

94 **a)** (Left) Mean GCaMP6s fluorescence change in I3 in response to 500 mM NaCl prior to and

95 following acclimation to 250 mM NaCl for 3 hrs. (Right) Peak fluorescence intensity changes

96 calculated from traces on the left. Each dot is the value from a single I3 neuron.

97 **b,d,e,g)** Percentage of animals of the indicated genotypes that are motile at each time point

98 following a shift from the acclimation plate (250 mM NaCl for 3 hrs) to 500 mM NaCl. Alleles

99 used were *flp-5(tm10075), flp-6(ok3056), flp-13(tm2427)*, *flp-18(db99), flp-18(tm2179), flp-*

100 *34(ok3071), nlp-3(tm3023), nlp-7(tm2984), nlp-10(tm6232), nlp-11(syb530), nlp-21(tm2569),*

101 *dmsr-1(sy1522), dmsr-7(sy1539), frpr-8(sy1362)* and *egl-6(n4537)*. Cre was expressed in I3

102 under the *glr-9* promoter. Each dot is the value from a single assay; n=30 animals per assay. *,

103 ** and *** indicate different from wild-type at the corresponding time at P<0.05, 0.01, and

104 0.001, respectively (one-way ANOVA and Dunnett's test). For e and g, wild-type and *glr-9* data

105 were interleaved, and are repeated.

106 **c,f)** Quantification of time to paralysis of animals of the indicated genotypes in the shown assay

107 conditions (cartoons at top (c) or left (f)). Each dot is the time at which all ten animals in a single

108 assay are immotile. Cre was expressed in I3 under the *glr-9* promoter. Control and experimental

109 animals were examined in parallel in the same assay.

110 The *glr-9(oy180)* allele was used in all experiments. Horizontal lines in all scatter plots indicate

111 the mean; errors are SEM. Data shown are from 2-3 independent experiments each. n.s. - not

112 significant.

113

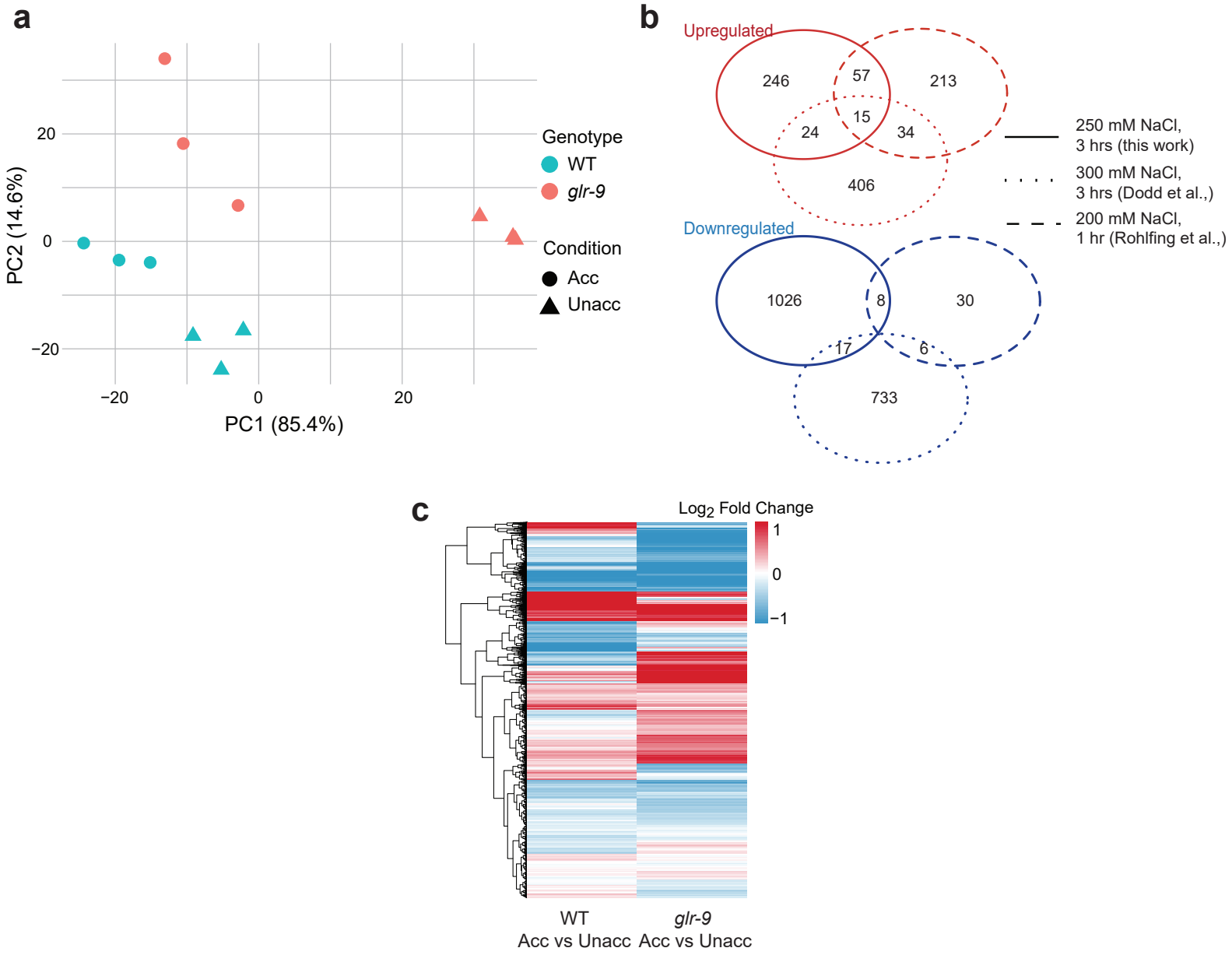

Yeon et al
Figure S5

114 **Fig. S5. Salt acclimation-induced changes in gene expression are partly regulated by GLR-**
115 **9-mediated signaling.**
116 **a)** Principal component analysis plot of RNA-Seq data clustered by genotype and condition.
117 Each data point is a single replicate.
118 **b)** Venn diagram showing overlap of differentially expressed genes between unacclimated and
119 salt acclimated wild-type animals identified in this and previously published work (Dodd et al.,
120 2018; Rohlfing et al., 2011).
121 **c)** A hierarchically clustered heatmap of all differentially expressed genes between acclimated
122 and unacclimated wild-type and *glr-9* mutants.
123 **d)** Volcano plots of differential gene expression between unacclimated and salt-acclimated wild-
124 type and *glr-9(oy180)* animals. Horizontal and vertical dashed lines indicate significant at
125 adjusted p-value <0.05 and $\log_2$ fold change >2 or <-2, respectively. A subset of genes involved
126 in osmotolerance and discussed in this work is indicated. Molecules categorized as being
127 involved in stress responses or metabolism, and in extracellular matrix remodeling, are indicated
128 in yellow and purple, respectively.
129

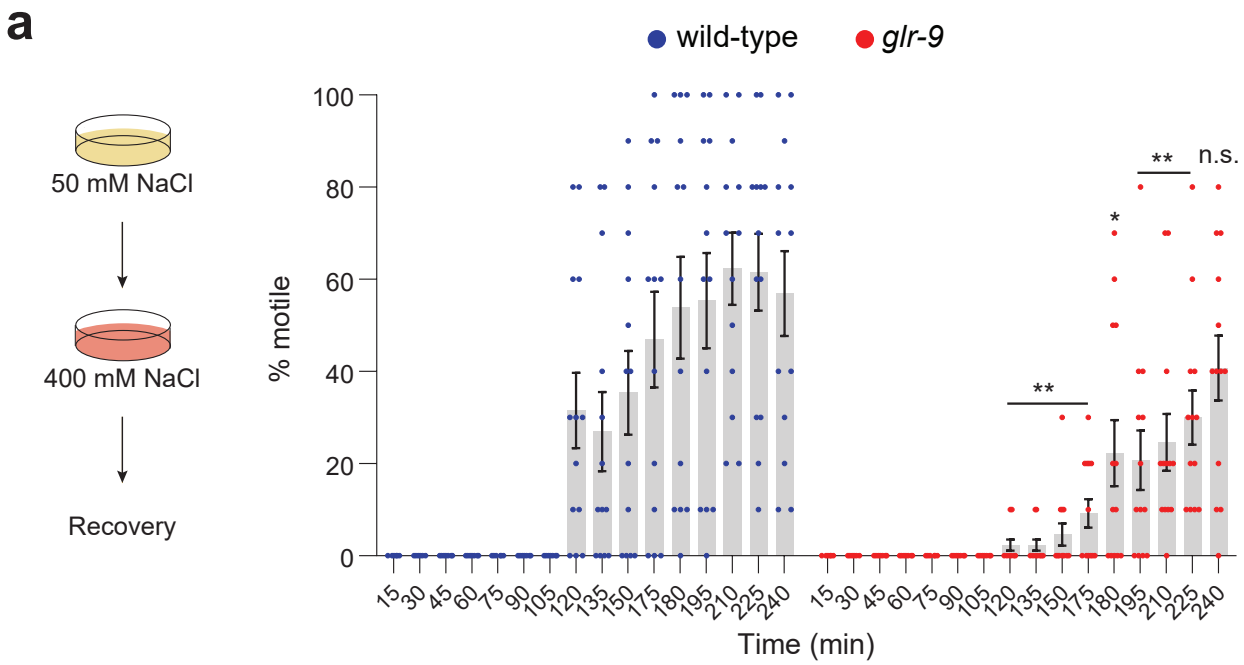

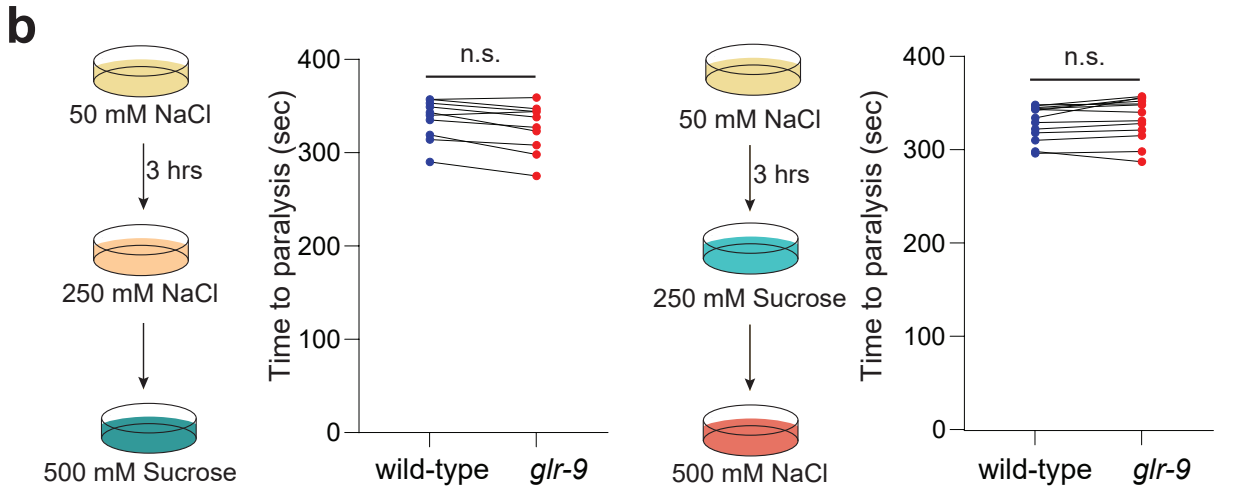

Yeon et al
Figure S6

130 **Fig. S6. *glr-9* mutants exhibit reduced recovery following salt stress.**

131 **a)** Percentage of wild-type or *glr-9(oy180)* mutants that are motile at each time point after being
132 moved from 50 mM NaCl to 400 mM NaCl. Each dot is the value from a single assay; n=10
133 animals per assay. * and ** indicate different from wild-type at the corresponding time at
134 P<0.05, 0.01, and 0.001, respectively (one-way ANOVA and Dunnett's test). n.s. – not
135 significant.

136 **b)** Quantification of time to paralysis upon shifting wild-type or *glr-9(oy180)* mutants acclimated
137 to 250 mM NaCl or 250 mM sucrose to 500 mM sucrose or 500 mM NaCl, respectively. Each
138 dot is the time at which all ten animals in a single assay are immotile. Wild-type and *glr-9*
139 mutants were examined in parallel in the same assay. n.s. – not significant.